Exploring Aqueous Fischer Tropsch Synthesis Using Unpromoted Cobalt-supported Catalysts

OLIVAS-RAMOS, EDER,NOE

Exploring Aqueous Fischer Tropsch Synthesis Using Unpromoted Cobalt-supported Catalysts

Eder Noé Olivas Ramos

MSc Thesis

Supervisors Dr Philip W. Dyer and Dr Simon K. Beaumont

Department of Chemistry, Durham University, UK

Contents

Acknowledgements

First and foremost, I would like to thank my supervisors, Dr Phil Dyer and Dr Simon Beaumont for their support and encouragement throughout the year. You have guided me with patience and taught me research skills that I'm continuously developing and will treasure for the rest of my career.

I would also like to thank Dr Emily Unsworth for her work on ICP-OES analysis and Dr Budhika Mendis for training me, with a lot of patience, on TEM analysis. Special thanks to Dr Benjamin Smith and Dr LiLi, for their guidance and help in the high-pressure laboratory.

To the amazing Dyer group; Alana, Ben, Claire, Dominikus, Jas, Kevin, Li Li, Mike (Michael H.), Michael (Michael L.), Stephen and those who have left the group, but I got to meet during the year (Anna, Ben, Jack, Kate, Leo and Sarah). I admire all of you. I have learned a lot from your work and I feel thankful that you accepted a chemical engineer into your group of crazy chemists. Thank you for showing me British culture in a science environment. Thank you for the laughs and the always interesting lunch conversations.

To my family; my mum, dad, my brother Irving and grandma Adela. You are with me every day. From the distance, I always feel your love and support.

Last, but certainly not least, thank you Daniel Whitehouse. Thank you for your company, your patience, your suggestions and your love. This experience would had never been the same without you.

Copyright notice

This thesis is based on work conducted by the author, in the Department of Chemistry at Durham University, during the period January 2017 to December 2017. All the work described in this thesis is original, unless otherwise acknowledged in the text or in the references. None of this work has been submitted for another degree in this or any other University.

Signed:_____ Date:_____

List of abbreviations

Å	Angström (10^{-10} m)
APFTS	Aqueous Phase Fischer Tropsch Synthesis
ARGE	Arbeitsgemeinschaft Ruhrchemie-Lurgi
bbl	Barrel
BOC	Birin's Oxygen Company
bpsd	Barrels per stream day
BTL	Biomass-to-liquids
CFB	Circulating fluidized bed
cm	Centimetre
COSHH	Control of Substances Hazardous to Health
CTL	Coal-to-liquids
FFB	Fixed fluidized bed
FID	Flame ionization detector
FTS	Fischer Tropsch Synthesis
g	Gram
GC	Gas chromatography
GTL	Gas-to-liquids
h	Hour
HTFT	High temperature Fischer Tropsh
i.d.	Internal diameter
ICP-OES	Inductively-coupled plasma-optical emission spectroscopic
IWI	Incipient wetness impregnation
K	Kelvin
L	Litre
LTFT	Low temperature Fischer Tropsch
m	Metre
mA	Milliampere
MFC	Mass flow controllers
min	Minute
mL	Millilitre
mm	Millimetre
MPa	Megapascal
o.d.	External diametre
ppm	Parts per million

Psi	Pounds per square inch
SAS	Sasol Advanced Synthol
SMR	Steam methane reforming
t	Tons
TCD	Thermal conductivity detector
vol	Volume
WGS	Water-gas shift
µm	Micrometre (10^{-6} m)

Abstract

A study of Aqueous Phase Fischer Tropsch synthesis (APFTS) is described whereby catalytic reactions were conducted using an aqueous suspension of a range of unpromoted, oxide-supported Co catalysts. The 5%-Co/SiO_2, 5%-Co/Al_2O_3, 10%-Co/SiO_2 and 25%-Co/SiO_2 catalyst samples were prepared *via* incipient wetness impregnation of the target support with cobalt nitrate. Optimizing the incipient wetness impregnation method led to the use of a packed column of the intended support through which an aqueous solution of cobalt nitrate was flushed under gravity. This gave a homogeneous material as confirmed by metal content analysis of portions of material extracted from along the length of the column using ICP-OES of acid-digested samples. In preparing an active Co-based supported catalyst for APFTS, an "*ex situ*" reduction proved to be a necessary step (350 °C at 5 °C / minute; H_2/N_2 50/50; flow rate 60 mL/min) after impregnation and calcination.

Catalyst samples of 5%-Co/SiO_2, 5%-Co/Al_2O_3, 10%-Co/SiO_2, 10%-Co/Al_2O_3 and 25%-Co/SiO_2 were tested for APFTS activity at 190 °C and 20 bar for 48 h. All of the catalysts showed a low activity, each forming carbon dioxide, methane, ethylene, and ethane as detected by gas chromatographic analysis of the reactor headspace. A catalytic activity for one of the more active catalysts reported (10%-Co/Al_2O_3) catalyst was determined to be 1 $\times 10^{-3}$ mol_{CO} $mol^{-1}{}_{Co}$ h^{-1}, calculated on the basis of the GC FID signal for methane. The catalytic activity reported is significantly low than that determined for either the 0.5%-Pt/25%-Co/Al_2O_3 and Co NP catalysts reported in the literature, something that is attributed to primarily intrinisic difference in the catalysts and also to the poor catalyst/gas contact in the batch reactor employed.

1. Introduction

Fischer Tropsch synthesis (hereafter FTS) is a well-established catalytic process in which a gas mixture consisting of carbon monoxide (CO) and hydrogen (H_2), commonly referred to as syngas, is used to produce liquid hydrocarbons such as paraffins and olefins, which find application in fuel production and chemicals, as well as oxygenates like alcohols, aldehydes, carboxylic acids, esters and aromatic compounds. FTS is achieved by passing syngas over a solid catalyst, typically cobalt- (Co) and iron- (Fe) based, at elevated temperatures and pressures. The overall FTS can be represented, simplistically, by the equations shown in Scheme 1.

$$nCO + (2n+1)H_2 \longrightarrow C_nH_{2n+2} + nH_2O$$

$$nCO + 2nH_2 \longrightarrow C_nH_{2n} + nH_2O$$

Scheme 1. Simplified overview of the reactions involved in FTS

FTS was first developed in the early 20th century, but since then has received increased recent interest as a consequence of environmental demands and technological developments. The syngas, the raw material for the FTS reaction, has traditionally been obtained through the gasification of non-renewable fossil fuels such as coal and natural gas.[1] However, today there is a shift away from the use of fossil-derived feedstocks, which have traditionally been employed for the production of transportation fuels, towards more sustainable friendly biomass resources (such as wood, agricultural wastes, organic wastes, *etc.*). This is achieved using a biomass-to-liquid process (BTL), which is regarded as a promising and carbon neutral alternative involving the gasification of biomass to yield a syngas suitable for FTS.[2] Biomass is a sustainable energy source in which the carbon dioxide emissions caused by its use are absorbed by newly-grown biomass, making this type of BTL process extremely attractive from an environmental point of view.

Despite the apparent simplicity of the FTS process, as will be discussed below, there is still considerable debate over the precise reaction mechanism by which it operates. Additionally, the FTS process is complicated by the fact that its sucess is extremely sensitive to the operating conditions, in particular whether it is being run as a gas/solid reaction (*e.g.* fluidised-bed, flow reactor, or fixed-bed reactor) or in the slurry phase (where syngas is bubbled through the waxy FTS products and finely-divided catalyst suspended in this liquid).[3–6] However, more recently in contrast to these conventional ways to perform the FTS reaction, where syngas is passed over a solid catalyst, recent studies have demonstrated that FTS can be undertaken in an aqueous suspension using various types of metal nanoparticle.[7] This alternative FTS approach has been called Aqueous Phase Fischer Tropsch synthesis (APFTS) and offers opportunities to re-examine this long-established process from various aspects. This includes probing the effects of catalytic supports, reactor design with facile product separation resulting from the immiscibility of the hydrocarbon products with water, and potentially the role of water in the reaction, since water is a co-product of FTS. Moreover, because FTS is a highly exothermic process, being able to perform the reaction at relatively low temperatures (facilitated by the high heat capacity of water) would be more thermodynamically favourable, potentially cleaner (by enhancing selectivity), and more environmental friendly as a result of the reduced energy input needed to achieve the reaction temperature.[7]

The work reported in this thesis will explore conducting APFTS using an un-promoted, supported Co catalyst to further investigate the chemistry of the catalytic process. This investigation includes a discussion of the preparation method for the catalyst, development of the test reactor, the catalytic testing, and the product analysis, together with method development.

1.1 General aspects of Fischer Tropsch Synthesis

Fischer Tropsch synthesis (FTS) is an example of a heterogeneous catalytic process, which is defined as a process in which the reactants are in a phase different from that of the catalyst. More specifically, FTS is a method by which synthesis gas, commonly referred to as syngas, which is a mixture consisting primarily of CO and H_2, is used to produce liquid hydrocarbons such as paraffins and olefins, as well as oxygenates like alcohols, aldehydes, carboxylic acids and esters. The necessary syngas is usually obtained through gasification of different fossil-derived sources such as coal, natural gas or biomass. The resulting gaseous mixture is often subject to reaction over a heterogeneous catalyst in order to modify the H_2:CO ratio to as near as possible to the desired 2:1 ratio necessary for FTS, a process known as the water-gas-shift (WGS) reaction – see Section 1.2.

Once syngas of an appropriate H_2:CO ratio is in hand, this gaseous mixture is passed over a heterogeneous catalyst at elevated temperature and pressure (for example, typical conditions being 220 °C, 30 bar[6]) to bring about FTS. Consequently, it is clear that one way of describing FTS is the hydrogenation of CO. In more detail, the reactions that can be used to describe the overall FTS process are shown in Scheme 1, which take place as a result of reactants adsorbing, dissociating, and reacting on the surface of the heterogeneous catalyst.[1,8]

$$nCO + (2n+1)H_2 \longrightarrow C_nH_{2n+2} + nH_2O \quad (1)$$

$$nCO + 2nH_2 \longrightarrow C_nH_{2n} + nH_2O \quad (2)$$

$$nCO + 2nH_2 \longrightarrow C_nH_{2n+2}O + (n-1)H_2O \quad (3)$$

$$nCO + (2n-1)H_2 \longrightarrow C_nH_{2n}O + (n-1)H_2O \quad (4)$$

$$nCO + (2n-2)H_2 \longrightarrow C_nH_{2n}O + (n-2)H_2O \quad (5)$$

Scheme 2. Generalised reactions involved in FTS.

From Scheme 2, the reactions (1) and (2) account for the formation of paraffins and olefins, respectively, while reactions (3), (4) and (5) account for the formation of synthetically versatile oxygenates. In regards to carbon chain growth, from the CO molecules to form hydrocarbon molecules, a sequence of steps occurs repeatedly on the catalyst surface. Hydrogen atoms are added to carbon and oxygen of CO, which results in the C-O bond splitting, and then compounds containing C-C and C-H forming. Taking the CH_2 group as an example, the following steps are necessary:[9]

- Associative adsorption of CO.
- Splitting of the C-O bond.
- Dissociative adsorption of $2H_2$ molecules.
- Transfer of 2H atoms to the oxygen to yield CH_2.
- Formation of a new C-C bond.

While the general, broad reaction is clear, a number of different mechanistic schemes have been developed to account for the observed FTS reaction chemistry. In this context, Bartholomew has noted that these mechanistic schemes can be grouped into three types, which differ in the ways in which CO is activated, how formation of monomer species occurs, and the way in which addition of monomer to growing chains takes place:[10]

i. The carbide mechanism.
ii. The hydroxyl-carbene mechanism.
iii. The carbonyl insertion mechanism.

A brief overview describing each of these processes will now be given.

1.1.1 The carbide mechanism

Franz Fischer is attributed as being the first person to make advances in proposing and understanding this FTS mechanism, after his results demonstrated that hydrocarbons could be the primary products of FTS (in his early results, oxygenates were the primary products). Consequently, Fischer, being aware of the tendency of Fe catalysts to form carbides, proposed CO-dissociation as the primary step in the FTS reaction mechanism and, consequently, iron carbides as intermediates.[9] These carbide species were proposed to be hydrogenated to methylene ("CH_2") groups. The resulting methylene groups were proposed to polymerize to form hydrocarbon chains that desorb from the surface as saturated and unsaturated hydrocarbons.[11]

Later, Craxford and Rideal proposed a more detailed carbide mechanism.[12] In their modified process, CO is adsorbed on the catalyst surface before dissociating in the presence of hydrogen, by forming water and CO_2, which rapidly desorbs leaving behind chemisorbed carbon at the surface. This surface carbon is subsequently hydrogenated to form chemisorbed CH_2 species, which oligomerize to produce higher carbon number hydrocarbons by the reactions shown in Scheme 3.[12]

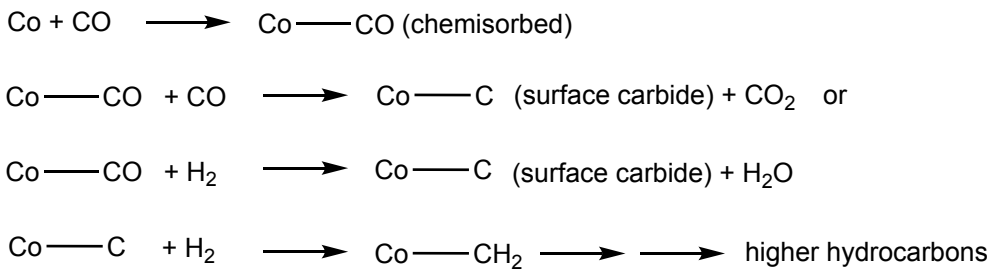

Scheme 3. Carbide mechanism proposed by Craxford and Rideal.[12]

Subsequently, Kummer *et al*. investigated the direct hydrogenation of the metal carbide.[13,14] Here, they pre-formed Fe carbide by the reaction of a reduced Fe

catalyst and then added radioactively-labeled ^{14}CO. The contribution of direct hydrogenation performed by Fe carbide can be measured by the fraction of $^{14}CH_4$ formed when the synthesis is effected with unlabeled CO. The results of their investigation showed that carbide hydrogenation could be responsible for no more than 8-30% of the methane formed. This study led most investigators to abandon the idea of the formation and subsequent hydrogenation of a bulk metal carbide as an intermediate in the FTS mechanism.[13,14]

1.1.2 The hydroxyl-carbene mechanism

In the 1950s, the hydroxyl-carbene mechanism (also described in literature as the oxygenate mechanism) gained widespread acceptance inspired by the oxygen-containing compounds formed in FTS, something proposed by Storch *et al.*[15] This mechanism involves the partial hydrogenation of adsorbed CO to an adsorbed hydroxycarbene (enol) species, and further hydrogenation to an alkene and water. When the chemisorbed CO reacts with adsorbed hydrogen the oxygenated species shown in Scheme 4 is formed.

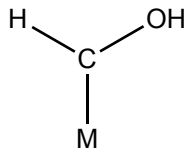

Scheme 4. Oxygenated species formed in the hydroxyl-carbene mechanism according to Storch *et al*.[15]

This functionality is formed from a combination of condensation and water elimination steps using adjacent surface-bound groups. This hydroxycarbene (enol) group can condense as depicted in Scheme 5.

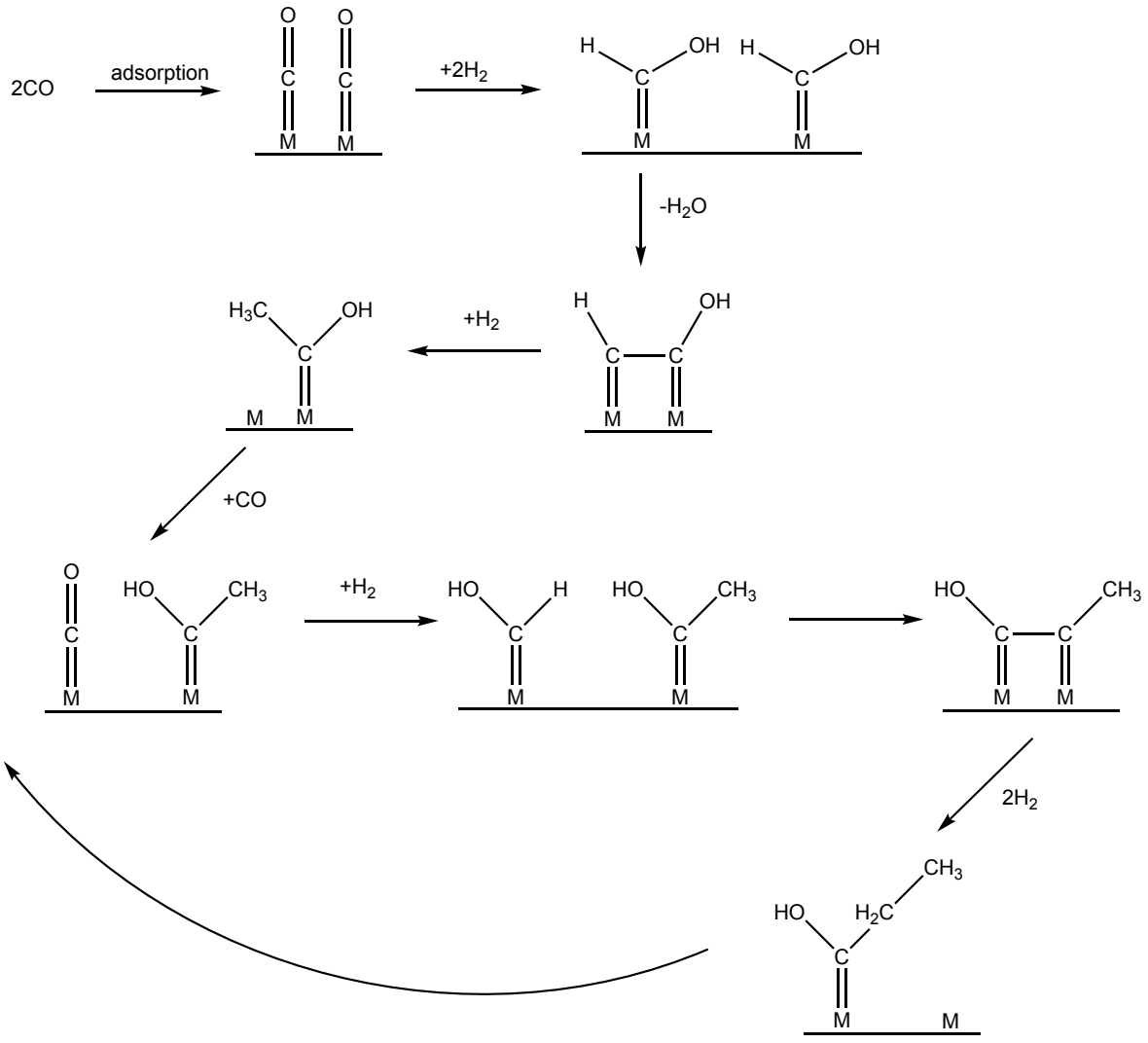

Scheme 5. Chain-growth mechanism for the hydroxyl-carbene mechanism modified from Davis, *Fuel Processing Technology*.[16]

Emmet *et al.* conducted studies adding ^{14}C-labeled alcohol or alkene to syngas to determine the distribution of the isotopically labeled products using an iron catalyst.[13] They found that the added alkene or the alcohol was able to serve to initiate chain growth. Since these studies were originally conducted at atmospheric pressure, more recently Davis, has conducted a similar study using medium pressure synthesis and slurry phase reaction conditions; the results obtained were in agreement with those of Emmett *et al*.[16]

By using surface chemistry techniques, no further support has been supplied for the hydroxyl-carbene mechanism that could prove the existence of the aforementioned hydroxycarbene (enol) species as proposed in Scheme 3. Furthermore, no support for the postulated condensation type of C-C bond formation by elimination of H and OH between adjacently adsorbed surface species to form water could be provided either, as initially proposed in Scheme 5. Therefore, since the hydroxyl-carbene mechanism has not been generally accepted, a different reaction mechanism, the carbonyl insertion mechanism, has been proposed as well. This mechanism will be further discussed in section 1.1.3.

1.1.3 The carbonyl insertion mechanism

The third FTS mechanism proposed, the carbonyl insertion mechanism, was postulated by Pichler and Schultz and is shown in Scheme 6.[9] It differs from the surface carbide mechanism (see section 1.1.1) only in the pathway leading to the formation of the adsorbed methylene group, which once formed, goes on to react in a way that resembles the CO insertion mechanism offered by Wender and coworkers.[11] This mechanism described by Pichler and Schultz involves the insertion of CO into a metal-methyl or metal-methylene, or metal-carbon bond, which is then hydrogenated to produce an alcohol or alkene; the alcohol or alcohol precursor can also eliminate oxygen to produce an olefinic product.

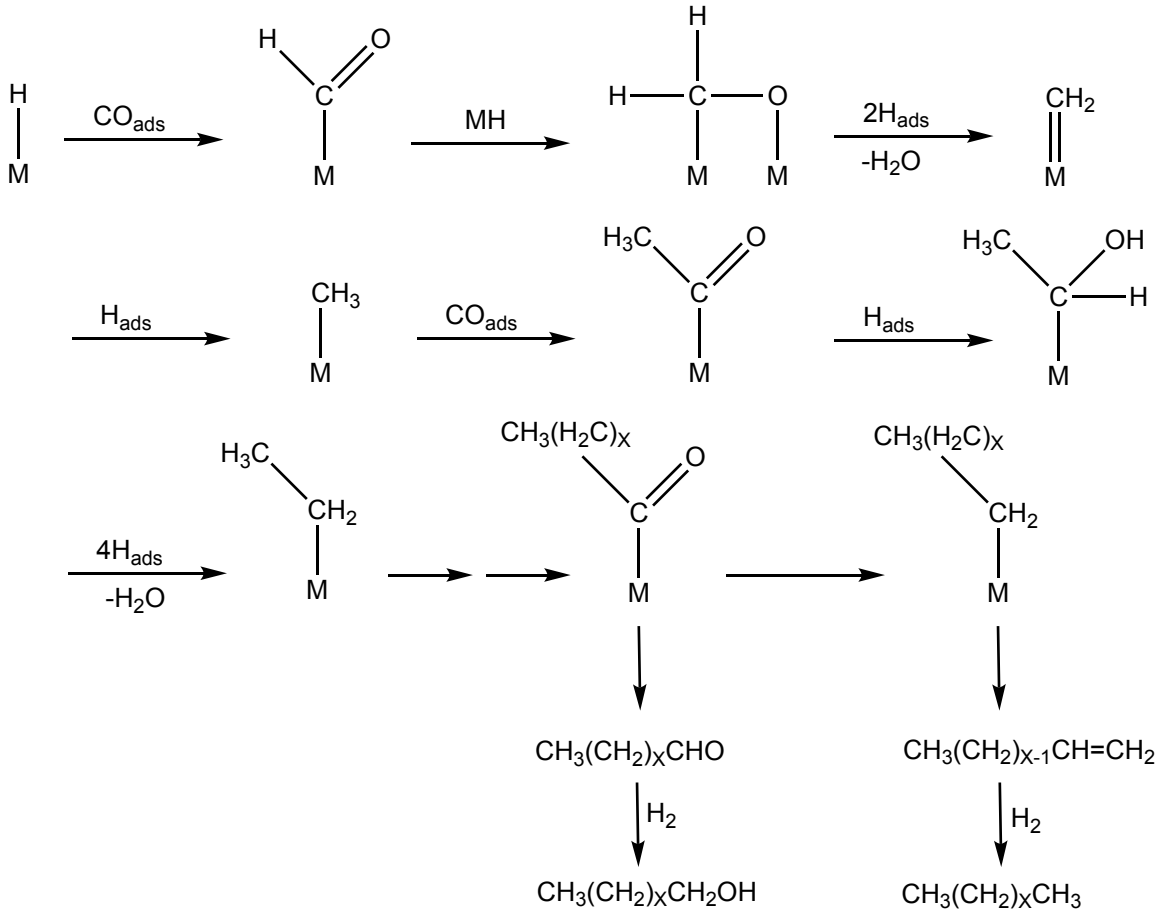

Scheme 6. CO insertion mechanism as proposed by Pichler and Schultz, modified from Davis, *Catalysis Today*.[11]

Observations made for the carbonyl insertion mechanism using surface science techniques showed an absence of oxygen on the catalyst surface, but an abundance of carbon, leading to the conclusion that CO chemisorbs and dissociates to adsorbed C and O.[11] This step is followed by the rapid hydrogenation of adsorbed O to produce water. In contrast, the hydrogenation of adsorbed carbon to form CH_2 is much slower. This led to the view that it was a surface, or near surface, metal carbide that was the initial surface species in the formation of carbenes.[11,16]

The fact that each of the mechanisms described above has and continues to attract considerable research and debate contrasts with the generally held belief that FTS can be regarded as a mature technology today, there remains no clear, definitive understanding of the mechanism that can be used to predict selectivity of the desired products for FTS. The nature of the process (and mechanism that is operative) is highly dependent on the catalyst selected to facilitate the synthesis, as well as the temperature and pressure conditions employed. These determining experimental factors will be further discussed in the following sections.

1.2 Industrial development of FTS.

The work of Sabatier and Senderens in the early years of the twentieth century showed that methane could be obtained catalytically from a mixture of CO and CO_2.[17] Subsequently, in 1926, Hans Fischer and Franz Tropsch published their work on hydrocarbon synthesis.[9] In this early work, they catalyzed the reaction of carbon monoxide and hydrogen over iron chips at a temperature of 673 K and a pressure above 100 bar, which lead to the formation of aliphatic oxygenated compounds that, when heated under a higher pressure still, produced a mixture of hydrocarbons. Later it was found that heavier hydrocarbons could be obtained directly by operating the process at a lower pressure of approximately 7 bar, which may be regarded as the advent of the FTS process.[18] The German company Ruhrchemie obtained the rights to this work, *i.e.* what is now known as the FTS process, and in 1936 the first plant using their technology in this area began operation.[6] Subsequently, the operating parameters have been changed throughout the industrial development process.

From an industrial perspective, FTS technology consists of three integrated operations: synthesis gas production, the FTS process, and the refining of products, as shown in Scheme 7.[19]

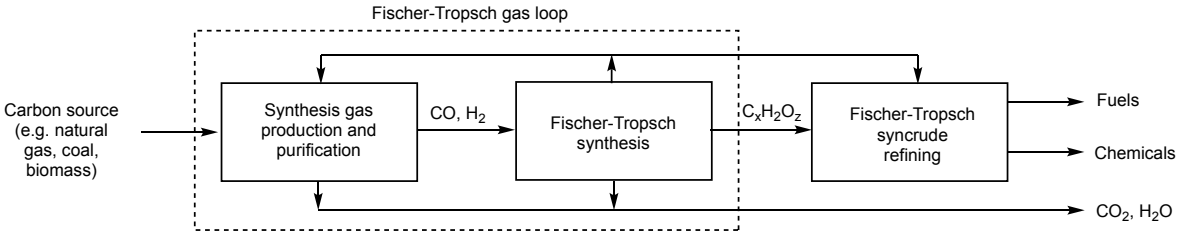

Scheme 7. General, simplified design features of an industrial FTS facility

A distinction between the different types of FTS facility being operated can be made according to the feed that is employed for the synthesis gas production, as described as the first step in Scheme 8. When the source of syngas corresponds to natural gas, the FTS plant is referred to as a gas-to-liquids (GTL) facility. When coal is gasified to produce synthesis gas, the facility is called coal-to-liquids (CTL).

For GTL plants the predominant commercial technology for syngas generation is steam methane reforming (SMR). This is a process in which methane gas and steam are catalytically and endothermically converted to hydrogen and carbon monoxide, producing a syngas mixture.[20] The process is conducted at high temperatures (700 - 1100 °C) using a Ni-based catalyst. The reaction is described in Scheme 8.[21]

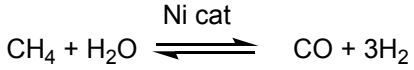

Scheme 8. Steam methane reforming reaction

The produced hydrogen is also used for the industrial synthesis of ammonia. Additional hydrogen can be recovered from the system with the application of the water-gas-shift reaction (WGS), producing carbon monoxide, in the presence of a Cu or Fe catalyst as shown in Scheme 9.

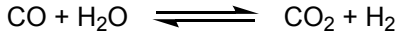

Scheme 9. Water-gas-shift reaction

In CTL technology, syngas is produced by coal gasification, which is a two-step process consisting of pyrolysis and char gasification.[22] The pyrolysis results in the evolution of compounds of low molecular weight, at temperatures between 300 and

500 °C. Typically, the pyrolysis residue, defined as char, represents from 55 to 70% of the original coal's original mass.

During the char gasification stage, the main reactions that take place can be described by those in Scheme 10.

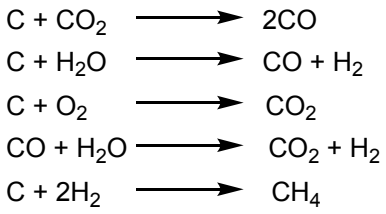

Scheme 10. Reactions describing char gasification

The syngas production in an FTS facility typically accounts for 60-70% of the capital and running costs of the total plant.[3] As a consequence, and given the availability of methane today, GTL technology is now the preferred option in comparison to CTL. The capital cost of the SMR facility is about 30% lower compared to coal gasification and overall, the process is more efficient. In SMR, about 20% of the carbon is converted to CO_2, whereas with coal gasification the conversion is about 50% due to coal's much lower hydrogen content. Since the cost of syngas is high, it is important that the maximum amount is converted in the downstream FTS reactors.

FTS technology is further classified according to its operation temperature: i) high-temperature Fischer-Tropsch (HTFT) and ii) low-temperature Fischer-Tropsch (LTFT).[18] The range of temperatures at which the HTFT process operates is 573-623 K. In HTFT typically the reactor of choice is of a fluidized bed design using an iron-based catalyst, which yields hydrocarbons in the C_1-C_{15} range. This process is

primarily used to produce liquid fuels, although a number of valuable chemicals, *e.g.* α-olefins, can also be extracted from the resulting crude synthetic oil. Oxygenates in the aqueous stream are separated and purified to produce alcohols, acetic acid, and ketones, including acetone, methyl ethyl ketone, and methyl isobutyl ketone. In contrast, for LTFT processes, the range of operating temperatures is typically 473-513 K. Here, both Fe- and Co-based catalysts are used to yield long-chain hydrocarbon waxes and paraffins, alongside high quality sulfur-free diesel fuels.[3,18] Most of the more recently implemented FTS technologies developed are based on the LTFT process. In the following table, the main FTS technologies that are in industrial operation are shown.[19]

Table 1. FTS technologies currently in industrial operation

Type	FTS catalyst	FT reactor type	FT technology	Operator	Commercial operation
HTFT	Fused Fe	Circulating fluidized bed	Sasol Synthol	PetroSA	Mossel Bay, South Africa
HTFT	Fused Fe	Fixed fluidized bed	Sasol Advanced Synthol (SAS)	Sasol	Secunda, South Africa
LTFT	Precipitated Fe	Fixed bed	ARGE*	Sasol	Sasolburg, South Africa
LTFT	Precipitated Fe	Slurry bubble column bed	Sasol Slurry Bed Process	Sasol	Sasolburg, South Africa
LTFT	Co-SiO_2	Fixed bed	Shell Middle Distillate Synthesis	Shell	Bintulu, Malasya
LTFT	Co-Al_2O_3	Slurry bubble column bed	Sasol Slurry Bed Process	Sasol	Ras Laffan, Qatar

*ARGE = Arbeitsgemeinschaft Ruhrchemie-Lurgi

Lastly, for the third and final stage of an FTS plant (Scheme 9), there is considerable variation in the design of commercial FTS refineries for product upgrading. Historically, both transportation fuels and chemicals were produced and the configuration of each refinery reflected the fuel specifications and chemical markets of its time. The carbon number distribution obtained during FTS is determined by the probability of chain growth on the catalyst, which is also called the α-value. The Anderson-Schultz-Flory (ASF) equation is often used to express the carbon number distribution.[19,23,24]

1.3 Catalysts used for Fischer Tropsch Synthesis

Vannice *et al.*[25] first reported the specific activities of Group VIII and IX metals supported on Al_2O_3 for FTS. In this context, it is possible to order catalysts based on the different metals employed with regards to the hydrocarbon chain length of the resulting products: Ru > Fe > Co > Rh > Ni > Ir > Pt > Pd.

Ruthenium-based systems are the most active for FTS, producing high molecular weight hydrocarbons at low temperatures.[3] However, ruthenium has a high cost and its worldwide availability is scarce, so its industrial application as an FTS catalyst is not practicable.[3] In contrast, both Co and Fe are commonly used as catalysts for FTS and offer a compromise between activity and cost.

In their review, Khodakov *et al*. presented a comparison of the different parameters such as cost, lifetime, activity at low conversion, water-gas shift reaction selectivity, *etc*. for Co and Fe catalysts.[18] This is summarised in Table 2.

Table 2. Comparison of Co and Fe catalysts in FTS. Table modified from Khodakov, *Chemical Reviews*.[18]

Parameter	Cobalt Catalysts	Iron catalysts
Cost	More expensive	Less expensive
Lifetime	Resistant to deactivation	Less resistant to deactivation (coking, carbon deposit, iron carbide)
Activity at low conversion	Comparable	
Productivity at high conversion	Higher; less significant effect of water in the rate of carbon conversion	Lower, strong negative effect of water on the rate of carbon monoxide conversion
Maximal chain growth probability	0.94	0.95
Water-gas shift reaction	Not very significant; more noticeable at high conversions	Significant
Maximal sulfur content	<0.1ppm	<0.2 ppm
Flexibility (temperature and pressure	Less flexible; significant influence of temperature and pressure on hydrocarbon selectivity	Flexible; methane selectivity is relatively low, even at 613 K
H_2/CO ratio	~2	0.5 – 2.5
Attrition resistance	Good	Not very resistant

Although Co-based catalysts are more expensive and toxic, they are more resistant to deactivation, having longer lifetimes FTS applications and are more resistant to attrition when supported on oxide supports, making them suitable for use in slurry-type reactors.[18] Although the catalytic activity at low conversion of Fe and Co systems is comparable, the productivity at higher conversion is more significant for cobalt catalysts. Water generated by FTS (Scheme 1) slows the reaction rate on Fe to a greater extent than on Co catalysts. This indicates that the WGS reaction (Scheme 10) is more significant for Fe. At relatively low temperatures (473-523 K), chain growth probabilities of about 0.94 have been reported for Co-based catalysts and about 0.95 for corresponding Fe systems.[5]

Both Fe- and Co-based catalysts are very sensitive to sulfur contamination. In this context, for Fe-based systems, it has been demonstrated that the syngas must not contain more than 0.2 ppm of sulfur. For Co catalysts, the amount of sulfur in the feed is required to be much less than 0.1 ppm to avoid poisoning.[3,4]. A distinctive characteristic of Co catalysts is that an increase in the operation temperature leads to a spectacular increase in methane selectivity, which is an undesirable product and this forces the FTS process to be operated within a very narrow range of temperatures and pressures. Generally, Fe catalysts are found to be more appropriate for conversion of biomass-derived syngas to hydrocarbons compared to their cobalt counterparts, because Fe systems can operate at lower H_2/CO ratios[18]. Based on the comparison of these different parameters for Fe- and Co-based systems, ideally a catalyst should be developed with the activity of a Co and the robustness of an Fe based catalyst towards changing operating conditions for its industrial application in FTS.

1.4 Types of reactor used in FTS facilities

Commercial reactors for FTS involve a number of different technologies.[18] Circulating fluidized bed and fixed fluidized bed reactors (CFB and FFB, respectively) are used for HTFT processes, which lead to gaseous products. In contrast, multi-tubular fixed bed and slurry reactors are dedicated to LTFT processes, which produce a large amount of wax in the liquid phase. Besides the intrinsic chemical kinetics of the FTS process, other phenomena have to be taken into consideration in order to choose the optimal reactor system, such as the heat transfer (FTS is highly exothermic), the hydrodynamics of flows, the mechanical stability of the catalyst, *etc*. The optimal industrial reactor should use a catalyst at its maximum capacity to convert the syngas and should achieve maximal hydrocarbon selectivities.[3]

A comparative analysis of the types of reactor used for the industrial operation of FTS can be made between HTFT and LTFT processes. For HTFT, an early example dates back to the 1950s, in a 5000 bpsd plant that operated briefly in Brownsville (Texas, U.S.A.), where commercial reactors of the FFB type were used to operate at conditions of 2.1-4.5 MPa and 305-345 °C. The syngas was produced from natural gas and an Fe-based catalyst was used. This combination yielded hydrocarbons rich in olefins, specifically α-olefins, while lower amounts of oxygenates and aromatics were also part of the products. The technology applied in this plant is referred in literature as the Hydrocol process.[6]

The HTFT technology applied by Sasol in South Africa is the largest commercial scale application of the Fischer-Tropsch technology. For the first Sasol plant at Sasolburg (South Africa), which began being constructed in 1952, CFB reactors were chosen to operate at about 2 MPa and 340 °C. For many years, these reactors presented good operating performance that, after some minor process and catalyst improvements, were named Synthol reactors.[3] In Sasolburg, coal gasification was originally used for syngas production, but a significant change

occurred in 2004 when this step was replaced by natural gas reforming, transforming the site into a GTL plant, then producing both waxes and chemicals.[6] In CFB reactors there are two fluidized catalyst phases. Catalyst moves down the standpipe in dense phase while it is transported up the “reaction” zone in lean phase as depicted in Figure 1 (A). To avoid the feed gas going up the standpipe, the differential pressure over the standpipe must always exceed that of the reaction zone. At high operating temperatures carbon is deposited on the iron-based catalysts, which lowers the bulk of the catalyst and thus the differential pressure over the standpipe.[3]

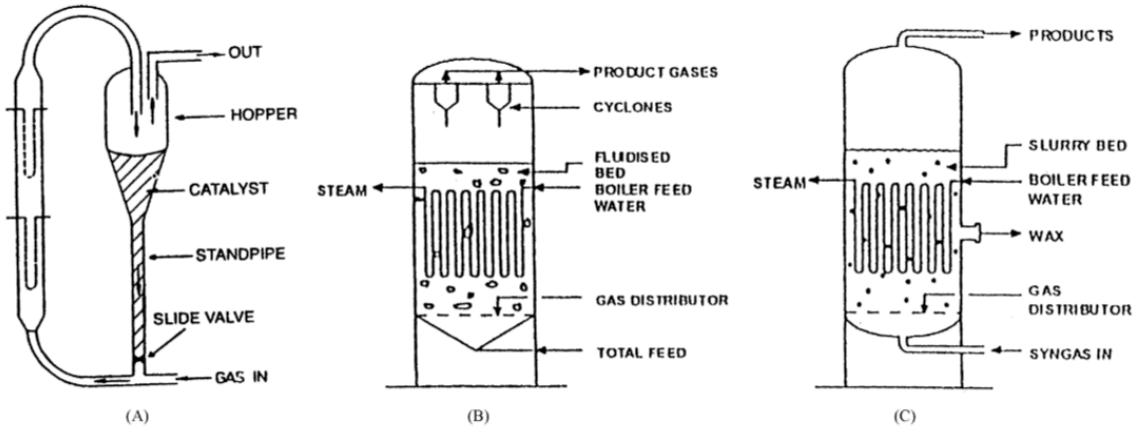

Figure 1. Fluidized bed FTS reactors: (A) CFB reactor, (B) ebulating or FFB reactor, (C) slurry phase bubbling bed reactor; figure modified from Dry, *Catalysis today*. Types (A) and (B) are two phase systems (gas and solid catalyst), while type (C) has three phases present, gas passing through a liquid in which the solid catalyst particles are suspended. Note the diagrams are not drawn to the same scale. The CFB reactors are about three times higher than the FFB or slurry reactors. [3]

The construction of the Sasol plant located in Secunda, South Africa, began in 1976 with a total of 16 Synthol CFB reactors, each with a capacity of 7500 bbl per day. From 1995 to 1999, these reactors were replaced by eight FFB reactors, four

of 8 m i.d. with capacities of 470×10^3 t per year each and four of 10.7 m i.d. each with a capacity of 850×10^3 t per year. These reactors were named Sasol Advanced Synthol (SAS) systems.[4,5]

The SAS reactor is a conventional fluidized bed designed to operate at ranges of pressure from 20 to 40 bar, which is typically operated at a temperature of around 340 °C using an iron catalyst similar to that used for the Synthol CFB reactors. The reactor consists of a vessel with a gas distributor, a fluidized bed containing the catalyst, cooling coils in the bed, and cyclones to separate entrained catalyst from the gaseous product stream.[3]

The main factor that distinguishes between the SAS and the Synthol reactors and that determines the relative conversion performance of the two types of Synthol reactors, is the quantity of catalyst that comes into contact with the feed gas in the reactor.[5] The catalyst/gas ratio in the reaction zone for the SAS reactor is about twice that for the CFB reactor. This is due to the fact that, although both reactors contain about the same quantity of catalyst overall, less than half of the catalyst in an CFB reactor is in the reaction zone; in an SAS reactor, the whole of the catalyst inventory is always in the reaction zone.[5]

Under the operating conditions typically used for LTFT, large amounts of liquid wax are produced, as previously mentioned, meaning that three phases are present in the reactor: liquid, solid (catalyst), and gas (syngas and products). In multi-tubular fixed bed reactors (fed from the top) the wax produced trickles down and out of the catalyst bed. In slurry reactors, the wax produced accumulates inside the reactors and so here the wax produced needs to be continuously removed from the reactor. An advantage observed for the slurry-phase reactors is that it tends to be well mixed due to the churning nature of the slurry-gas bubble interaction, making it isothermal and giving place to a better and more flexible temperature control. On

average, the operating temperatures can be higher than in multi-tubular fixed bed reactors, eliminating the danger of carbon formation and break-up of catalyst. At higher average conversions, a better control of selectivities can be achieved.[5]

For the first Sasolburg FTS plant, the HTFT process was combined with the use of five multi-tubular ARGE reactors (LTFT) that were installed for wax production. These reactors still operate at 2.7 MPa and 230 °C and the production capacity of each is about 21×10^3 t per year.[6]

In the Shell plant in Bintulu (Malaysia), constructed in 1993, there are four large multi-tubular reactors each with a capacity of about 125×10^3 t per year, with around 10,000 tubes per reactor. As Co-based catalysts are used in these units, which are much more reactive than the Fe-based catalysts used in the Sasolburg reactors, the tube diameters of the Shell reactors are narrower in order to cope with the higher rate of reaction heat released.[3]

As for the use of slurry bed reactors for FTS, several investigators studied the process in the 1950s, *e.g.* Kölbel developed and operated a 1.5 i.d. unit. In the late 1970s Sasol R&D compared the performance of fixed- and slurry-bed systems in their 5 cm i.d. pilot plants and found the conversions and selectivities to be similar.[3] In 1993 a 5 m i.d. commercial unit was commissioned by Sasol and has been in operation ever since. Its capacity is about 100×10^3 t per year, which equals that of the combined production of the original five ARGE reactors. Using a cobalt-based catalyst Exxon successfully operated a 1.2 m i.d. slurry bed reactor for wax production. The capacity of this unit was 8.5×10^3 t per year.[3]

1.5 Cobalt-based Fischer Tropsch Synthesis

Because of their stability, higher per-pass conversion, and high hydrocarbon productivity, Co-based catalysts represent the optimal choice for synthesis of long-chain hydrocarbons in the LTFT process (excess of CH_4 is produced at high temperatures since Co is a more hydrogenating catalyst and overall, the products are more hydrogenated than those produced by Fe-based catalysts).[5] The production of liquid hydrocarbons over a cobalt catalyst was first reported in 1913.[26] In the subsequent decades, catalyst science and technology involved has advanced from a simple cobalt oxide supported on asbestos to sophisticated, high activity, highly-optimized cobalt catalyst system supported on carefully-modified supports and promoted with noble metals and basic oxides.[26] Because of the high price of Co (at least compared to that of Fe) it is desirable to minimize the amount of metal used, but to maximize the available surface area of the metal. To achieve this the Co is dispersed on high stability supports such as Al_2O_3, SiO_2 or TiO_2.[3]

In their review, Khodakov *et al*. state that there is a consensus in the literature that FTS proceeds at cobalt metal particles.[18] The attribution of catalyst FT activity to Co metal phases has been built on a series of experimental findings. Indeed, it has been found that unsupported metallic cobalt and cobalt monocrystals are active in FTS.[27] Cobalt metallic phases were always detected in the active catalyst before, during and even after FTS. Iglesia *et al.* showed that for large cobalt metal particles, the reaction rate is proportional to the number of cobalt surface sites.[28–31] Based on these findings, it can be suggested that FTS is a structure-insensitive reaction, for cobalt-based systems at least.

The synthesis of highly dispersed Co catalysts requires the initial formation of very small CoO or Co_3O_4 crystallites. The formation of these small oxide clusters in turn requires strong interactions between the oxide support and the Co precursor for their stabilisation. However, such interactions tend to interfere with the low-temperature reduction of such precursors to Co metal. On strongly interacting

supports (*e.g.* Al_2O_2), high reduction temperatures are required, which leads to extensive agglomeration and to the formation of large Co metal particles. In contrast, cobalt precursors can be readily reduced on weakly interacting supports (such as SiO_2), but such supports are unable to stabilize very small precursor crystallites during impregnation and drying. Thus, optimum cobalt dispersions are favoured by support-precursor combinations with intermediate interaction strengths.[32]

1.5.1 Synthesis of Co-based catalysts for FTS

The catalytic performance of FTS catalysts is very much influenced by the preparation method of the catalysts. The preparation of Co-supported catalysts involves several important steps including: the choice of appropriate catalyst support; the choice of method for deposition of the active phase (Co metal particles); inclusion of catalyst promoter; and the oxidative and reductive treatments employed.[18] These critical factors for FTS catalyst preparation will be analyzed in the following sections.

1.5.1.1 Support role and influence of support texture

The principal function of the catalyst support is to disperse cobalt and to produce stable cobalt metal particles after reduction. The porous structure of the support is believed to exert a controlling effect on the size(s) of supported cobalt particles.[18] Supports are also beneficial with regards to the exothermic characteristic of FTS since they provide a pathway for dissipating the heat released by the reaction and thus, reducing temperature gradients that would result in fixed bed reactors. The support could affect the structure and electronic properties of small cobalt metal particles and also, it could react with Co species forming Co-support mixed compounds.[33]

Additionally, the support modifies the mechanical strength of FTS catalysts. The catalyst solidity (mechanical strength) is a crucial issue for slurry FTS reactors. The acidity of the catalyst support leads to olefin isomerization, lower chain growth probability, and higher selectivity to ligher hydrocarbons.[34]

The importance and potential role played by the support in FTS is emphasized by the fact that several reports have focused on the effect of the support in such processed. Reuel and Bartholomew conducted studies on the catalytic activities and selectivities of unsupported and supported Co catalysts measured at low conversions and conditions of 1 atm and 175 – 350 °C. It was found that the activity for supported catalysts as a function of the support declines in the following order: Co/TiO_2 > Co/Al_2O_3 > Co/SiO_2 > 100%Co > Co/MgO.[35] Iglesia *et al.* found that at pressures greater than 5 bar and at high conversions, the influence of the support on the selectivity in the formation of CH_4 and C_{5+} hydrocarbons was insignificant.[29]

The effects of Co SiO_2- and Al_2O_3-based systems will be further discussed in the following sections.

1.5.1.1.1 Silica-supported catalysts

The support-metal interaction between SiO_2 and Co is relatively weak in SiO_2-supported catalysts. This aspect usually leads to a better reducibility of immobilized Co-containing species. At the same time, Co dispersion is much lower for SiO_2-supported catalysts than for Al_2O_3-supported ones. Thus, the major challenge in the design of SiO_2-supported catalysts is to achieve a high Co dispersion, something that would allow the ready cobalt reduction to be exploited.[18]

Studies on the effect of texture of SiO_2-supported catalysts of different pore diameters conducted by Saib *et al*. showed that a catalyst supported by SiO_2 with an average pore diameter of 10 nm (100 Å) was most active and selective for C_{5+} hydrocarbons.[36] Song and Li also reported similar results for a series of Co catalysts supported on SiO_2.[37] Catalysts with pore size of 6-10 nm displayed higher FTS activity and selectivity towards C_{5+} hydrocarbons. It was also observed that with increasing pore size of the support, the interaction of the Co oxide species with the support became weaker and that the dispersion of the catalyst decreases when increasing pore size of the support.

1.5.1.1.2 Alumina-supported catalysts

Al_2O_3 has been one of the most used supports for cobalt FTS catalysts. There is a strong support-metal interaction between Al_2O_3 and Co oxides leading to the formation and stabilization of small cobalt crystallites. A reaction between the small Co particles and the support can result in diffusion of the cobalt active phase into the bulk Al_2O_3, thus forming Co aluminate spinels, which is not beneficial for the catalytic process.[38,39] However, cobalt reducibility remains one of the most important problems of Al_2O_3-supported cobalt FTS catalysts, although promotion with noble metals can improve this (see section 1.5.1.3). Several methods have been used to improve the properties of alumina supports for FTS, including using a pretreatment of the Al_2O_3 before the active phase deposition.[18] For example, Zhang *et al.* reported that pre-treatment with acetic acid has a negative effect on Al_2O_3 supports, while reactions with ammonia and ammonium nitrate presents an improvement in the catalytic behaviour.[40] In their studies, Zhang *et al*. found that the existence of acetate and a high number and strength of acid sites increases the interaction between Co and support, which then leads to the lower reducibility of catalysts. Cobalt catalysts supported on alumina and ammonium nitrate-treated alumina with a lower number of acid sites showed higher reducibility and more bridged-form Co structures, which can be the main cause for the high activity.[40] Another pre-treatment approach focused on coating Al_2O_3 with a protective layer: studies conducted by Li *et al.* demonstrated that small amounts of magnesia added by impregnation on an Al_2O_3-supported Co catalyst improves the activity and increases the olefin to paraffin ratio, but larger amounts of magnesia decrease the activity.[41] Li *et al*. found that that the large amounts of magnesia restrained the reduction of the catalysts due to the formation of an MgO-CoO solid solution.

The support texture represents another tool to control the structure, dispersion, and reducibility of Co particles. A larger size of support pores generally leads to larger Co_3O_4 crystals.[18] Studies conducted by Bechara *et al*. showed the importance of the porosity of catalyst pellets after impregnation on the activity and selectivity for FTS.[42]

1.5.1.2 Deposition of Active Phase by Incipient Wetness Impregnation

The goal of active phase deposition is to spread Co species throughout a porous support, which ultimately will provide the precursors of the necessary pre-catalytic Co metal clusters. Co-supported catalysts for FTS are very often prepared by impregnation. Impregnation techniques can be classified by the nature of the metal precursor used for deposition; Co salts and Co carbonyls are the common precursors. In this report, only Co salt precursors are going to be investigated experimentally. For catalysts prepared *via* impregnation and decomposition of Co salts, reduction of the Co species is necessary. This step will be further discussed in section 1.5.1.4.

Incipient wetness impregnation (IWI) is the most common used method to prepare Co-supported catalysts. In the IWI method, a solution of a Co salt, typically cobalt nitrate (due to its high solubility and ease of decomposition of the anion – albeit generating unwanted NO_x), is contacted with a dry porous support. After the contact, the solution becomes dispersed inside the pores of the support as a result of capillary forces. The incipient wetness impregnation is complete when all pores of the support are filled with the liquid and there is no excess moisture over and above the amount of liquid required to fill the pores. Although at the first sight the practical execution of IWI is simple, the fundamental phenomena underlying impregnation and drying are extremely complex. Reproducible synthesis of Co catalysts requires careful control of all impregnation parameters, such as the temperature and time of support drying, the rate of addition of impregnating solution, temperature and time drying, *etc.*[18] Additionally, if the volume of solvent to just fill the pores is incorrectly judged and excess solvent is present, the rate of dispersion of the cobalt-containing solution throughout the oxide material will be slowed, as a result of becoming reliant on simply just diffusion.

The initial distribution of cobalt on the support depends to a large extent on the type and concentration of hydroxyl groups on the surface and pH of impregnating

solution.[43] At the stage immediately after impregnation, the interaction between the metal precursor and the support is relatively weak, thereby allowing redistribution of the active phase over the support body to occur during drying and calcination.

The distribution of Co^{2+} ions (from the Co salt) on the support after impregnation is affected by electrostatic interactions. Porous oxides such as Al_2O_3, SiO_2 and TiO_2 have different points of zero charge (PZC).[44] At pH below the PZC, the surfaces of the corresponding oxides are charged positively; at pH higher than the PZC, the surface of the support is charged negatively. If the impregnating solution has pH below the PZC, repulsion between the surface of the support and Co^{2+} atoms results in non-homogeneous repartition of cobalt ions. At pH higher than the PZC, Co^{2+} cations are distributed much more homogenously. However, elevated solution pH can lead to dissolution of the support in the impregnating solution.

The concentration, distribution, and nature of the hydroxyl groups of the support also play an important role in the genesis of the dispersion of supported metal. The concentration of these hydroxyl groups can be controlled by pretreatment of the support with organic compounds, such as those mentioned in section 1.5.1.1.2, and through addition of tetraethylorthosilicate. Zhang *et al*. investigated the effect of pretreatments with acetic acid, 1-propanol, and 1-butanol on a SiO_2 support before impregnation. In the studies of Zhang *et al*. better activity and a higher Co dispersion was found due to solvents modifying the surface properties of SiO_2, thus enhancing Co dispersion and reducibility simultaneously.[45]

1.5.1.3. Effect of promoters on the catalytic activity of Co-based systems

The introduction of a noble metal (Ru, Rh, Pt, and Pd) has a strong impact on the structure and dispersion of Co species, FTS reaction rates, and catalytic selectivities.[18] Co-based catalysts promoted with noble metals are typically prepared *via* co-impregnation of porous supports with an aqueous solution of a cobalt salt and noble metal precursors such as perrhenic acid, ruthenium nitrosyl nitrate, tetraammineplatinum(II) nitrate, *etc*. Noble metals as promoters can have the following effects on the catalyst: i) much easier reduction of cobalt oxide particles, ii) formation of bimetallic particles and alloys, iii) a lower fraction of barely reducible mixed oxides, iv) enhancement in cobalt dispersion, v) inhibition of catalyst deactivation, vi) appearance of additional sites of hydrogen activation, and vii) an increase in the intrinsic reactivity of surface sites.[18]

A significant effect of promotion with noble metals on the number of Co metal sites has been observed on Al_2O_3-supported catalysts. For example, the reduction temperature of Co oxides decreases to lower values with the addition of Pt and Ru as promoters.[46,47] Studies conducted by Tsubaki *et al*. have shown that the addition of a small amount of Ru to Co catalysts increases the extent of cobalt reduction, whereas addition of Pt and Pd species as promoters does not have any effect on cobalt reducibility.[48] The catalytic activity was determined for different promoted catalysts and was shown to follow the order: CoRu > CoPd > CoPt > Co. It was found by Tsubaki *et al*.that the catalysts promoted with Pd and Pt exhibited higher CH_4 selectivity.[48] Shimura *et al*. studied the promotion effect of thirteen metals (Mg, Ca, Sr, Ba, Y, La, Ce, Ti, V, Mn, Zn, Zr and Mo) on an Al_2O_3 support and it was found that V, Mn and Mo decreased Co reducibility and surface area of Co metal.[49]

Re has a less significant promotion effect than either Pt and Ru. The reduction of Co_3O_4 to metallic cobalt proceeds *via* intermediate formation of CoO. It has been suggested that the presence of Re affects only the second reduction step, from

CoO to Co. This has been attributed to the fact that reduction of Re occurs above the temperature of Co_3O_4 to CoO reduction.[50]

FTS catalyst promotion with noble metals can also affect the decomposition of the Co-containing precursor, which is often a simple Co salt, as described in section 1.5.1.2. Girardon *et al*. have reported that promotion using ruthenium nitrosyl nitrate results in a lower temperature of decomposition of cobalt acetate and a higher density of cobalt metal sites in the resulting catalyst.[51]

Enhancement in Co dispersion is another effect due to introduction of noble metals to cobalt catalysts. One of the reasons responsible for the higher cobalt dispersion can be related to a higher concentration of cobalt oxide nucleation sites during decomposition of cobalt precursors in the presence of promoting noble metals. A higher concentration of Co_3O_4 nucleation sites (at the same cobalt content) can result in a larger number of cobalt particles and consequently higher cobalt dispersion in the catalysts.

Oxides can also be used as promoters, with ZrO_2, LaO_3, MnO, and CeO_2 being the most employed.[18] The effects of oxides as promoters are: i) a modification of the catalyst texture and porosity; ii) decrease the formation of hardly reducible Co mixed oxides; iii) increase Co dispersion; iv) reducibility, and fraction of different Co metal crystalline phases; v) enhancement of mechanical and attrition resistance of Co catalysts; and vi) improvement in the chemical stability of the support.[18]

1.5.1.4. Effect of catalyst oxidizing and reducing pretreatments on cobalt dispersion and reducibility

Cobalt precursor decomposition is an important stage in catalyst preparation. The heat released during decomposition of cobalt precursors can affect the structure of cobalt species in the final catalysts.[18]

The work of Girardon *et al*. showed that the decomposition of cobalt nitrate in air at 423 K is slightly endothermic when supported on SiO_2.[52] Here supported cobalt ions agglomerate into Co_3O_4 crystallites or react with SiO_2, producing amorphous cobalt silicate. Due to the endothermicity of cobalt nitrate decomposition, this formation of Co_3O_4 crystallites is favored. At relatively low temperatures, the endothermic decomposition of cobalt nitrate leads to higher Co dispersion, but decreases Co reducibility.

A much smaller effect of the temperature of decomposition of cobalt nitrate on cobalt dispersion was observed for Al_2O_3-supported cobalt catalysts as reported by Wigzell *et al*. The decomposition/reduction behavior of cobalt nitrate hexahydrate supported on Al_2O_3 and SiO_2 in two gas atmospheres was investigated. During the decomposition of cobalt nitrate hexahydrate under an oxygen/argon atmosphere, NO is the major decomposition product, with the decomposition being described at 350 °C by the equation in Scheme 11.[53]

$$3\left[Co(NO_3)_2 \bullet 6H_2O\right] \longrightarrow Co_3O_4 + 6NO + 18H_2O + 4O_2$$

Scheme 11. Decomposition of cobalt nitrate hexahydrate under oxygen/argon atmosphere

Typically, the reduction of the Co oxide spinels (Co_3O_4) occurs in two steps: Co^{+3} to Co^{+2} and Co^{+2} to Co^0, as illustrated in the following Scheme 12.

$$Co_3O_4 + H_2 \longrightarrow 3CoO + H_2O$$

$$CoO + H_2 \longrightarrow Co + H_2O$$

Scheme 12. Co oxide reduction steps

The study of Wigzell *et al*. revealed that in an oxygen/argon atmosphere, simulating a calcination atmosphere, the decomposition of cobalt nitrate is generally simplified in comparison with the unsupported salt with fewer weight loss events measured by TGA.[53] When supported on Al_2O_3, cobalt nitrate is stabilized with decomposition events shifted to higher temperatures, whereas when supported on SiO_2, cobalt nitrate is destabilized with only one significant decomposition event, which occurs at a lower temperature. In a hydrogen/nitrogen atmosphere (*i.e.* a reducing atmosphere), partial decomposition of cobalt nitrate occurs before reduction is initiated over both supports. When supported on Al_2O_3, cobalt nitrate reduction is catalyzed with the two events below 350 °C happening at lower temperatures, while the reduction that takes place above 350 °C is pushed to higher temperatures. In contrast, the SiO_2-supported complex exhibits reduction events that are all reduced in temperature relative to the unsupported salt. However, there is evidence of the formation of cobalt silicate with a high-temperature reduction.[53] The study also showed that the calcination and direct reduction of supported cobalt nitrate is significantly affected by the support and that different conditions are required to achieve the same state.[53]

1.5.2 Effect of water on cobalt-based FTS

Water is the primary oxygen-containing product of FTS. For Co-based catalysts, the oxygen atoms are predominantly removed as water. This water can affect the syngas conversion, hydrocarbon selectivity, FTS product distribution and catalyst longevity. These effects can be observed due to the influence of water on the degree of syngas adsorption on the catalyst, chain initiation, chain growth, methanation, hydrogenation to paraffins, and dehydrogenation to olefins.[54] Methane is an undesirable product since it is of low value (compared to the FTS starting materials) and its formation occurs at the expense of more desirable hydrocarbon products. From an economic perspective, recycling the methane formed in FTS by converting it back into syngas *via* SMR is not favourable. The effects of water on syngas conversion and catalyst deactivation are determined by the FTS reaction mechanism. As described in sections 1.1.1, 1.1.2 and 1.2.3, the reaction mechanism is considerable complex and there is no consensus as to a definitive mechanism.

Dalai and Davis reviewed the effects of water on the performance of unsupported and supported Co catalysts.[54] The amount of water formed depends upon CO conversion, reactor system, and catalyst used. As described in Section 1.3, Co catalysts do not exhibit a significant WGS activity and by increasing the CO conversion and residence time, the water partial pressure increases. For fixed bed reactors, the water partial pressure increases gradually along the reactor, whereas for slurry type reactors, the water concentration is homogeneous and it is desirable for CO conversion to be maintained high during which water concentration approaches saturation level.[54]

It was also outlined by Dalai and Davis that in the case of supported catalysts, the extent of the effect of water on catalytic performance depends on the amount of water present in the catalyst as well as the presence of noble metal promoters.[54] The addition of water in FTS decreases/increases CO conversion; CH_4, C_{+5}

hydrocarbons, olefins and CO_2 selectivities depending on the Co loading, support and promoter and the trend in selectivities often depend on the process conditions.[54] In general, for SiO_2 water effects are positive in the case of higher CO conversions, whereas for Al_2O_3 the effects are negative as deactivation is observed due to surface oxidation or the oxidation of small cobalt crystallites.[54]

1.5.3 Aqueous Phase Fischer Tropsch Synthesis

Aqueous Phase Fischer Tropsch Synthesis (APFTS) operates under the same principle as FTS, namely by converting syngas into hydrocarbons. However, in APFTS the reaction is catalyzed in the presence of liquid water in which the catalyst is suspended or dissolved.

Chao-Xian *et al*. first reported APFTS in 2007.[7] Their initial work was based on the report that soluble nanoclusters in ionic liquids or liquid water exhibit good catalytic activity performance in the hydrogenation of various organic substrates.[55–59] Chao-Xian *et al*. conducted studies catalyzing FTS using different solvents for the reaction, such as [BMIM][BF_4], ethanol, dioxane and cyclohexane to dissolve water-soluble Ru nanoclusters with a diameter of 2.0 ± 0.2 nm stabilized by poly(*N*-vinyl-2-pyrrolidone) (PVP). When adding water to ethanol in the system, a significant enhancement in activity was observed. By conducting the synthesis in pure liquid water an unprecedented activity of 6.9 $mol_{CO}mol_{Ru}^{-1}h^{-1}$ was achieved, a value that was almost 35 times that achieved using a Ru/SiO_2 catalyst. The APFTS tests were conducted by sealing the syngas (3.0 MPa, H_2/CO = 2:1) in a stainless-steel autoclave running in batch mode at 150 °C along with a catalyst suspended in water. This is considered the first report of APFTS and offers new opportunities to re-examine the well-established FTS catalytic process. The work reported by Chao-Xian *et al*. showed that Ru nanoclusters in the absence of any support show a higher activity than that of supported catalysts. This finding suggests that a reconsideration is necessary of the effects of supports on catalysts used for FTS. APFTS also offers the opportunity to employ a reactor system with the advantages of a slurry type reactor, as described in section 1.4, due to an easier product separation. This separation occurs due to the immiscibility of the hydrocarbon products and the water-soluble catalyst. However, due to the high cost of Ru, alternative options, such as Co-based systems, have to be explored for possible industrial application of APFTS.[7]

Queck *et al.* conducted APFTS using Ru nanoparticle catalysts dispersed in water with an average size of 2.2 ± 0.3 nm at 30 bar (H_2/CO ratio = 2).[60] An unprecedented aldehyde selectivity up to 70% (dominant product) was obtained at a temperature of 125 °C. The authors suggested that reaction temperature strongly affects the relative rates of different termination mechanisms and that hydrocarbon and oxygenate formation occur on different reaction sites of Ru nanoparticles with hydrocarbons being formed on sites with a low barrier of CO dissociation.[60]

Lingtao *et al*. have conducted APFTS using a continuous flow reactor, which is a crucial step for the feasibility demonstration in an industrial consideration. Ru nanoparticles reduced by hydrogen in the presence of PVP showed the highest activity compared to those particles reduced by other reactants. With a PVP/Ru molar ratio of 40 and a particle size of 2.0-2.2 nm, an almost steady space time yield (STY) of C_{5+} hydrocarbons (0.51 g-C_{5+}g-cat^{-1}h^{-1}) was kept for 240 h running at 150 °C. It was suggested that the PVP/Ru molar ration and reaction temperature are two key factors for the stability and activity of the catalysts.[61]

As stated in Section 1.3, a main drawback of using Ru-based catalysts is their high cost. Consequently, APFTS has also been conducted using Co-based catalysts, which are more suitable for industrial application. Wang *et al*. conducted APFTS using Pt-Co nanoparticles at 160 °C, with a low loading of Pt (molar ratio of Pt:Co = 0.05)[62]. It was observed that when Pt was introduced during a one-step hydrogen-reduction preparation of the catalyst, the activity increased to 0.6 mol_{CO}•$mol_{Co}^{-1}h^{-1}$, around one order of magnitude higher than that of the pure Co catalyst and even comparable to Co catalysts working at higher reaction temperatures.[62] The selectivity towards unwanted products, CH_4 and CO_2, dropped dramatically (CH_4: 10%; CO_2: 2%), while those towards C_{2-5} and C_{5+} changed to 17% and 70% respectively. This report gave indication that the addition of Pt over the Co nanoparticles could greatly improve the reaction rate of the catalysts.

Co-supported catalysts have also been reported for APFTS. Pendyala *et al*. studied the effect of reaction temperature of a Ru nanoparticle catalyst in comparison with supported Ru and Co catalysts. Under similar activation and reaction conditions (3.0 MPa for 24 h in a 1L stainless steel autoclave in the batch mode operation), the activity of the supported (Ru or Co) catalysts was reported to be lower than the Ru nanoparticle catalyst and CO_2 formation is high for supported catalysts.[63] The synthesis was conducted at 125, 145 and 165 °C. On increasing the reaction temperature, oxygenate selectivity decreased and the corresponding hydrocarbons selectivity increased. The activity of the supported Co catalyst (0.5% Pt-25%Co/Al_2O_3) was found to be low. As for product selectivities for this catalyst, hydrocarbons are the predominant products (67 %) and oxygenate selectivity was around 11% with the remaining being carbon dioxide (22%). This selectivity suggested that at least a part of the Co had been oxidized to an oxide phase that is active for WGS.[63] The authors suggested that the soluble Ru nanoparticle catalysts are freely rotational and three dimensional in APFTS reaction systems. Thus, their metal-surface active sites are much more accessible for the reactant molecules here, which is responsible for their high activity.

1.6 Project Aims

In exploring the chemistry of APFTS, this project will focus on the impact of different stages that constitute the catalytic process; the catalyst preparation, the catalytic testing and the gas and liquid phase products analysis.

Despite a high activity value of 6.9 mol_{CO} mol_{Ru}^{-1} h^{-1} having been reported by Chao-Xian *et al*.[7] using Ru nanoparticles, so far, APFTS has not been reported using unpromoted Co-supported catalysts, which is crucial for the understanding of the chemistry of the reaction. Consequently, here a Co-based system will be employed in this thesis, since Co is a more suitable catalyst for the industrial application of FTS (section 1.3).

As reported by Pendyala *et al*., APFTS has been conducted using a 0.5%Pt-25%Co/Al_2O_3 catalyst.[63] It is of high interest to understand the effect of the Pt promoter by using an unpromoted Co-supported catalyst. Moreover, Pendyala *et al*. prepared the Pt promoted catalysts using a slurry impregnation, however, the incipient wetness impregnation method is conventionally the method used for Co-based catalysts for FTS. Therefore, the preparation method of the catalyst will also be explored.

The results obtained will be used for comparison with reports in literature for APFTS described in the previous section, in an attempt to better understand the chemistry of this synthesis.

2. Experimental

2.1 General Experimental Considerations

All glassware was oven-dried before use. Unless stated otherwise chemicals were obtained from Sigma Aldrich or Alfa Aesar and were used without further purification. Evonik Aeroperl 300/30 fumed silica (described herein as SiO_2) and Alfa Aesar γ-alumina (1/8" pellets ground and sieved to <250 μm; described herein as γ-Al_2O_3) were used as catalyst supports. Deionised water was used throughout.

Ar, CO, H_2 and N_2 (all from BOC) were passed through scrubbing columns containing $CaCl_2$, alumina and carbon for Ar; sodalime, alumina, carbon and Cu/Zn for CO; and alumina, carbon and Cu/Zn for H_2.

Inductively coupled plasma-optical emission spectroscopic (ICP-OES) analyses were carried out by Dr. E. Unsworth (Durham University).

Laboratory coat and safety spectacles were worn at all times and gloves as appropriate; all experiments were conducted in an efficient fume-hood, following completion of appropriate COSHH and risk assessments. Solvents and solid residues were disposed of in the appropriate waste receptacles (chlorinated/non-chlorinated), with aqueous heavy metal-containing residues being classified according to metal.

2.2 Preparation of cobalt-based catalysts

2.2.1. Preparation of silica-supported cobalt catalysts via incipient wetness impregnation using a round bottom flask

The SiO_2-supported cobalt catalysts (5%Co/SiO_2 and 10%Co/SiO_2) were prepared *via* an incipient wetness impregnation method using $Co(NO_3)\cdot 6H_2O$ (0.548 g) dissolved in water (1.85 mL). In a disposable weighing boat, Evonik Aeroperl 300/30 fumed silica SiO_2 (1.0 g) was weighed and then transferred into a round bottom flask placed on top of a cork ring. The metal precursor solution was then added drop-wise using a syringe to the oxide support. After impregnation, the round bottom flask was connected to a rotary evaporator for initial water removal

under reduced pressure. The samples were transferred to a petridish using a spatula and then dried in an oven at 110 °C for 12 h. Finally, the samples were calcined at 350 °C (ramp rate of 100 °C/h) for 4 h under an oxygen/nitrogen atmosphere (20/80).

2.2.2 Preparation of silica-supported cobalt catalysts via incipient wetness impregnation using a plastic syringe

The SiO_2-supported cobalt catalysts (5%Co/SiO_2, 10%Co/SiO_2 and 25%Co/SiO_2) were prepared *via* an incipient wetness impregnation method using $Co(NO_3)\cdot 6H_2O$ (0.548 g) dissolved in water (1.85 mL). In a disposable weighing boat, Evonik Aeroperl 300/30 fumed silica SiO_2 (1.0 g) was weighed, but for this method, the oxide support was transferred into the barrel of a 10 mL plastic syringe. The syringe barrel was securely clamped with the tip at the bottom and closed at the tip with glass wool. A glass vial was placed underneath the syringe for metal precursor solution collection, in case of dripping. The Co-containing precursor solution was then added drop-wise from the top using a syringe. After 12 h, the samples were transferred to a petridish using a spatula and then dried in an oven at 110 °C for 12 h. Finally, the samples were calcined at 350 °C (ramp rate of 100 °C/h) for 4 h under an oxygen/nitrogen atmosphere (20/80).

2.2.3 Preparation of alumina-supported cobalt catalysts via incipient wetness impregnation using a round bottom flask

The Al_2O_3-supported cobalt catalysts (5% Co/Al_2O_3 and 10%Co/Al_2O_3) were prepared *via* incipient wetness impregnation method using $Co(NO_3)\cdot 6H_2O$ (0.548 g) dissolved in water (0.75 mL). In a disposable weighing boat, previously ground and sieved Al_2O_3 (1.0 g) was weighed and then transferred into a round bottom flask placed on top of a cork ring. The metal precursor solution was then added drop-wise using a syringe to the oxide support. After impregnation, the round bottom flask was connected to a rotary evaporator for initial water removal under reduced pressure. The samples were transferred to a petri dish using a spatula

and then dried in an oven at 110 °C for 12 h. Finally, the samples were calcined at 350 °C (ramp rate of 100 °C/h) for 4 h under an oxygen/nitrogen atmosphere (20/80).

2.2.4 Preparation of alumina-supported cobalt catalysts via incipient wetness impregnation using a plastic syringe

The Al_2O_3-supported cobalt catalysts (5% Co/Al_2O_3, 10%Co/Al_2O_3 and 25%Co/Al_2O_3) were prepared *via* incipient wetness impregnation method using $Co(NO_3)\cdot 6H_2O$ (0.548 g) dissolved in water (0.75 mL). In a disposable weighing boat, previously ground and sieved Al_2O_3 (1.0 g) was weighed, but for this method, the oxide support was transferred into a 10 mL plastic syringe with the plunger removed. The syringe was securely clamped with the tip at the bottom and sealed at the tip with glass wool. A glass vial was placed underneath the syringe for metal precursor solution collection, in case of dripping. The Co-containing precursor solution was then added drop-wise from the top using a syringe. After 12 h, the samples were transferred to a petri dish using a spatula and then dried in an oven at 110 °C for 12 h. Finally, the samples were calcined at 350 °C for 4 h (at a rate of 100 °C/h) under an oxygen/nitrogen atmosphere (20/80).

2.3 Metal content analysis by inductively coupled plasma-optical emission spectroscopy (ICP-OES)

The ICP-OES instrument (Jobin Yvon Horiba Ultima 2) was calibrated for cobalt concentration over an appropriate range using a commercial standard. Additionally, control samples were prepared by dissolving an authentic sample of $Co(NO_3)\cdot 6H_2O$ in ultra-high purity water and averaged over two runs to identify systematic errors. All experimental ICP-OES data are reported for the calibrated cobalt concentration.

2.3.1 Acid digestion of Co-based catalysts using glass vials

The mass of samples was calculated as well as an appropriate volume in which to dilute the sample to achieve a measurable concentration for analysis. The mass of samples and standard solution was weighed into glass vials using a balance. In a fume cupboard, an oil bath was set on top of a hotplate. A glass vial containing only water was securely clamped so most of the exterior of the vial was in contact with the oil. The hotplate contact thermometer probe was clamped so that the end was in the vial containing only water to monitor the temperature. In a fume cupboard, a solution of *aqua regia* was prepared (1:3 HNO_3:HCl, both concentrated) in a measuring cylinder. *Aqua regia (*5 mL) was added to each sample and the standard solution and each of the vials securely clamped in an oil bath. The samples were heated for 3 h by setting the temperature on the hot plate at 85 °C and stirring to medium. The samples were then allowed to cool to room temperature. Volumetric flasks for each sample were partially filled with ultra-high purity water. The contents of each vial containing the samples after acid digestion was transferred to the corresponding volumetric flask. Each vial was rinsed with water three times and the washings were then added to the corresponding volumetric flasks. Each volumetric flask was made up to the mark with water. Using a pipette, approximately 10 mL of each solution was transferred to ICP sample tubes. The sample tubes properly marked with each catalyst sample and the standard compound were submitted for analysis.

2.3.2 Acid digestion of Co-based catalysts using test tubes

The methodology for the acid digestion using test tubes was the same as described in section 2.3.1, but in this case 20 cm-long test tubes were employed to contain the catalyst samples and the standard compound.

2.4 Cobalt-based catalysts characterization by transmission electron microscopy (TEM)

Transmission electron microscopy studies were conducted using a JEOL 2100F FEG transmission electron microscope with a Schottky field emitter operating at 200 kV. A resolution of 2.3 Å (1 Å information limit) was used for TEM imaging. The catalyst samples were ground and dispersed in ethanol using an ultrasonic bath. Three drops of the suspension were then placed on a porous carbon film and air-dried.

2.5 *Ex situ* reduction for Co-based catalysts

In addition to the "*in situ*" reduction, which will be described in section 2.6, an "*ex situ* reduction" was explored for the cobalt-based catalysts. Here, after the samples were prepared according to the protocols presented in sections 2.2.1, 2.2.2, 2.2.3 or 2.2.4, each material was transferred into a reduction tube (fused quartz). The tube was heated to 350 °C at 5 °C / minute inside a furnace and under a hydrogen/nitrogen (50/50) atmosphere at a flow rate of 60 mL/min.

2.6 Catalytic testing

A schematic of the reactor setup is presented in Figure 2 and a picture of the actual reactor system in Figure 3. The reactor consists of a 15 mL stainless steel tube with an internal diameter (i.d.) of 10 mm and external diameter (o.d.) of 12 mm, sealed at one end with a stainless steel cap held in place with a compression fitting (Hamlet). Surrounding the bottom of the reactor tube there is a stainless steel split aluminium block (i.d. 12 mm, o.d. 40 mm) around the reaction zone, which is surrounded by a band heater (200 W) attached to a temperature and process PID controller box (Omega CN7500). The reactor tube sits on top of a stirrer hotplate used only for stirring in conjunction with a Teflon-coated cross-type magnetic stirrer bar located inside the reactor tube.

At the top of the reactor tube, there is a gland fitting sealed with an annealed copper gasket. The top of the gland fitting is connected to a ½"-to-¼" tubing reducing union (Hamlet compression fitting), which then connects to a cross-piece. One arm of the cross-piece is connected to a safety pressure relief valve (PRV) set at 51.5 bar. The top arm has a K-type thermocouple attached, which passes through a sealing gland compression fitting such that the tip of the thermocouple is located in the reaction solvent. The last arm of the cross piece connects to a T-piece fitted, *via* compression fittings (Hamlet), to a pressure transducer (range 0-60 bar, output 4-20 mA, manufacturer), which then connects to a second T-piece with a pressure gauge (100 bar) before then going through a ¼"-to-$^{1}/_{8}$" reducing union connected to a third T-piece. Attached to this T-piece is an outlet needle valve, which is used for reaction sampling when connected to GC equipment. On the other arm, there is an inlet needle valve with a preceding check valve ($^{1}/_{3}$ psi) to prevent reverse gas flow during reactor pressurization/gas feeding. Gases are fed into the reactor *via* a gas manifold connected to external cylinders.

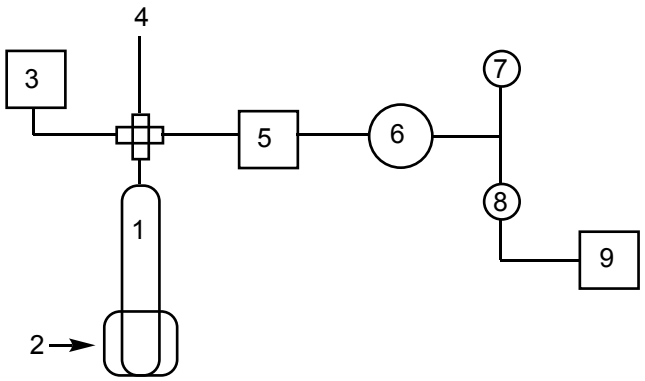

Figure 2. Reactor system used for catalytic testing of APFTS: 1) reactor tube, 2) band heater, 3) relief valve, 4) thermocouple, 5) pressure transducer, 6) pressure gauge, 7) outlet needle valve, 8) inlet needle valve, 9) gas manifold.

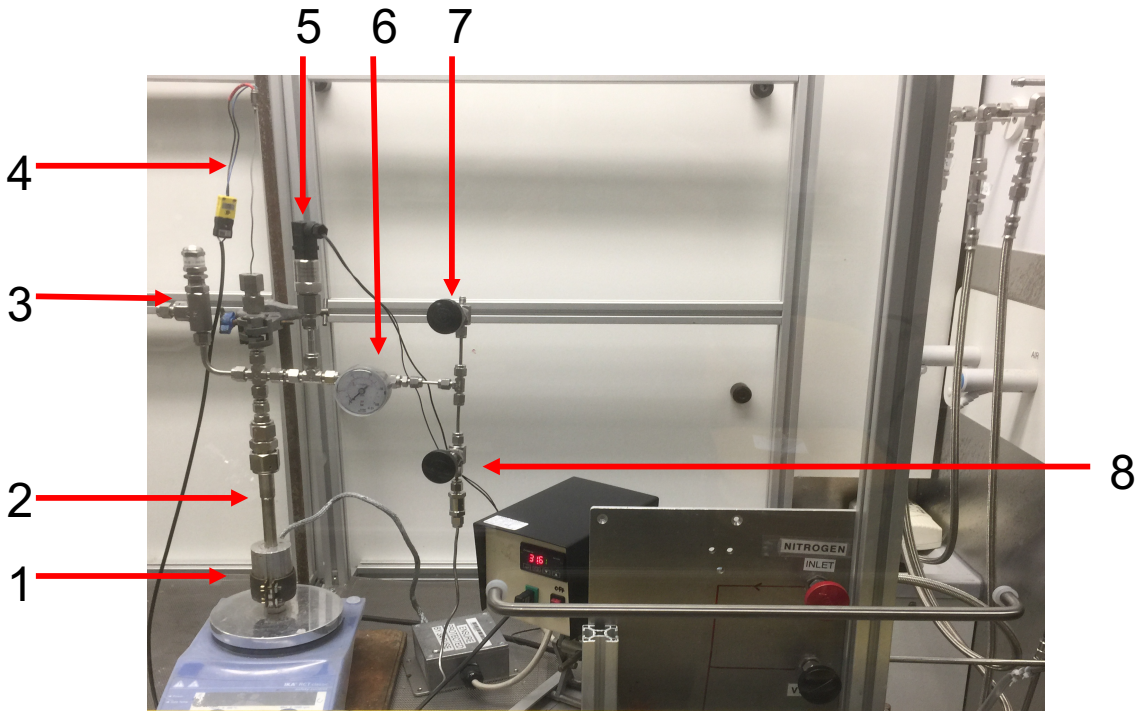

Figure 3. Picture of the reactor system used for catalytic testing of APFTS with components as labelled in Figure 2.

Aqueous phase Fischer Tropsch Synthesis (APFTS) was carried out in the reactor tube fitted with a Teflon-coated cross-style magnetic stirrer bar in a fume cupboard. To this end, a suspension of the desired catalyst (200 mg) in ultra-high purity water (5 mL) was prepared and added into the reactor, taking care that all solids were transferred. The reactor was flushed with H_2 gas three times (14 bar) and sealed under a pure H_2 atmosphere (14 bar, room temperature). The reactor was then heated to 150 °C at 8 °C / minute (as monitored by an internal K-type thermocouple) with stirring (using the magnetic stirrer bar), and the temperature then held at 150 °C for 2 h in order to achieve an "*in situ*" reduction of the catalyst before catalytic testing. After allowing the reactor to cool to room temperature, the reactor was flushed with Ar gas three times (2 bar) and sealed under a mixture of Ar (2 bar), CO (6 bar), and H_2 (12 bar). The reactor was then heated to 190 °C at 10 °C / minute (as monitored by an internal K-type thermocouple) with stirring and this temperature then held for 48 h. After this time the reactor was allowed to cool

to room temperature and the products were analyzed according to the method described in section 2.7.

2.7 APFTS Organic Product Analysis

Any organic products arising from APFTS were analyzed by Gas Chromatography (GC - Bruker SCION^{TM} 456, fitted with both a flame ionization {FID} and a thermal conductivity {TCD} detector). A shin carbon ST 100/120 packed column (2 m × 1 mm i.d. × 1/6 in o.d. silica) was used for analysis of permanent gasses (Ar, H_2, and CO) and gas products. A capillary column (Agilent technologies, 30m × 0.250 mm, 0.25 μL coating thickness) was used for liquid products analysis. Helium (BOC cp grade) was used as a carrier gas and TCD balance gas. Hydrogen was used for the FID detector, produced using a Peak Scientific hydrogen generator (40 psi), fed to the GC *via* a combined oxygen and moisture trap.

2.7.1 Gaseous Products Analysis Protocol

After catalytic testing described in section 2.6, the inlet needle valve (component 8, Figure 3) was disconnected from the filling line, allowing the reactor system to be moved next to the gas chromatography equipment. The outlet needle valve (component 7, Figure 3) was connected to a flow meter using a 70 cm-long (o.d. $^1/_8$ in.) tube, which was in turn connected to the GC inlet sampling loop (1 mL) using a 70 cm-long (o.d. $^1/_8$ in) tube. By carefully opening the outlet needle valve, the gas was allowed to flow at a rate of 20 mL/min into the GC sample loop for 2 min and then, the GC analysis programme was then run. The GC heating protocol was as follows: starting point of the temperature program was set at 45 °C. Then, the oven temperature was increased to 250 °C at a rate of 20 °C/min and it was held for 15 min. The GC was used to obtain the retention times and area peaks for C_1-C_5 paraffins, Ar, H_2, CO and CO_2.

2.7.2 Liquid Product Analysis

To verify the presence of liquid APFTS products, analysis was conducted by extraction of any liquid organic products from the aqueous phase with diethyl ether (5 × 3 mL), with the resulting ethereal solution then being analyzed by GC. This was achieved by injecting the liquid product sample into the Bruker SCION^{TM} 456 GC using a dedicated autosampler. The injection volume was 1 μL and the split ratio was 20:1. A flame ionization detector (FID) was used for this analysis. The starting point of the temperature program was set at 40 °C. Then, the oven temperature was increased to 240 °C at a rate of 20 °C/min where it was held for 10 min.

2.7.2.1 GC Liquid Organic Product Calibration

A study was undertaken to validate the extraction methodology and detection limit sensitivity of the organic products in the aqueous phase and calibration of the GC equipment using different concentrations of cyclohexane dissolved in diethyl ether.

Solutions of volumes of 100, 75, 50 and 25 μL of cyclohexane diluted in diethyl ether (3 mL) were prepared in vials. Each solution was analyzed by GC-FID. The injection volume was 1 μL and the split ratio was 20:1.

2.7.2.2 Extraction of liquid products from APFTS reaction mixtures

After catalytic testing, the reactor tube was detached from the gland fitting. The liquid phase was poured from the reactor tube into a centrifuge tube. The sample was then centrifuged at a speed of 8000 rpm. The liquid phase was separated from the solid products using a plastic pipette and was transferred into a vial. This liquid phase was mixed with 3 mL of diethyl ether and the solution was transferred to a separating funnel. The solution was extracted three times with diethyl ether (3 mL), the washings being combined, before being analyzed by GC-FID.

2.8 Catalytic conversion and catalytic activity calculations

To calculate the conversion rates for H_2 and CO using the retention times and peak areas from the chromatograms obtained, Ar was used as a reference (tie gas) since it is unreactive for APFTS. The GC equipment was calibrated using mass flow controllers (MFC, Brooks Delta Smart 2, 0-50 sccm) to flow various known mixtures of gasses (Ar, H_2 and CO) and determine their retention times and area peaks by GC to produce percentage calibration curves for each gas, referenced to Ar.

The MFC flows were calibrated for each of the gasses using a bubble flow meter. The set point was varied for each gas and the actual flows were measured to produce calibration curves for each MFC. From the calibration curves, for each gas set point (nominal flow), the real flow (actual flow) can be obtained. The calibration curves obtained can be observed in Figures 4, 5 and 6.

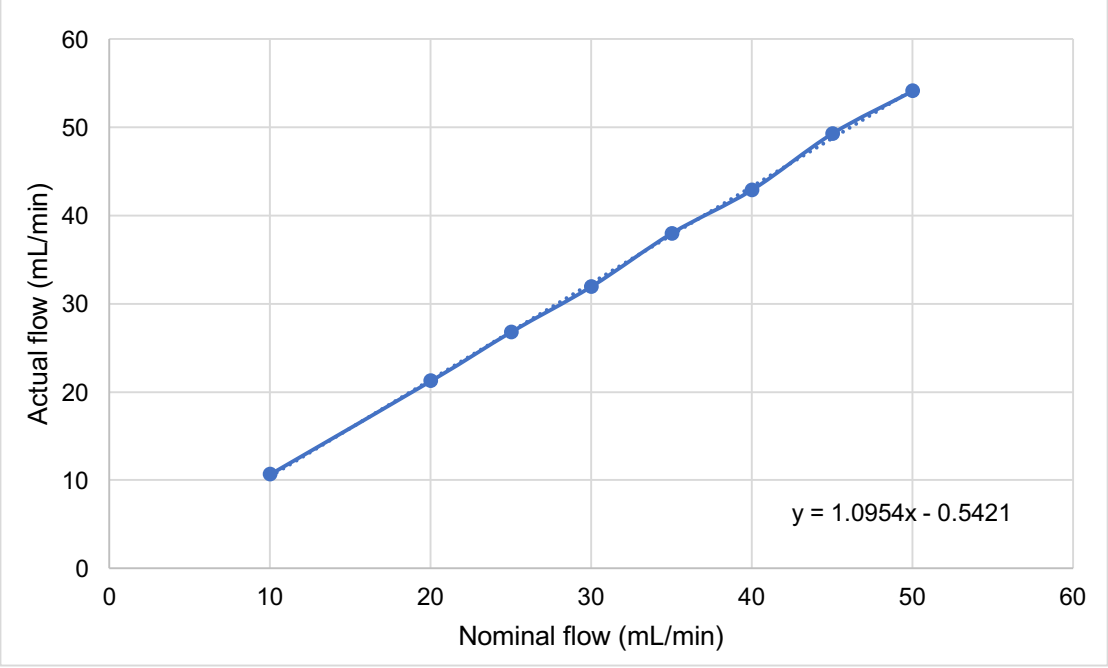

Figure 4. Experimentally-determined argon MFC calibration curve

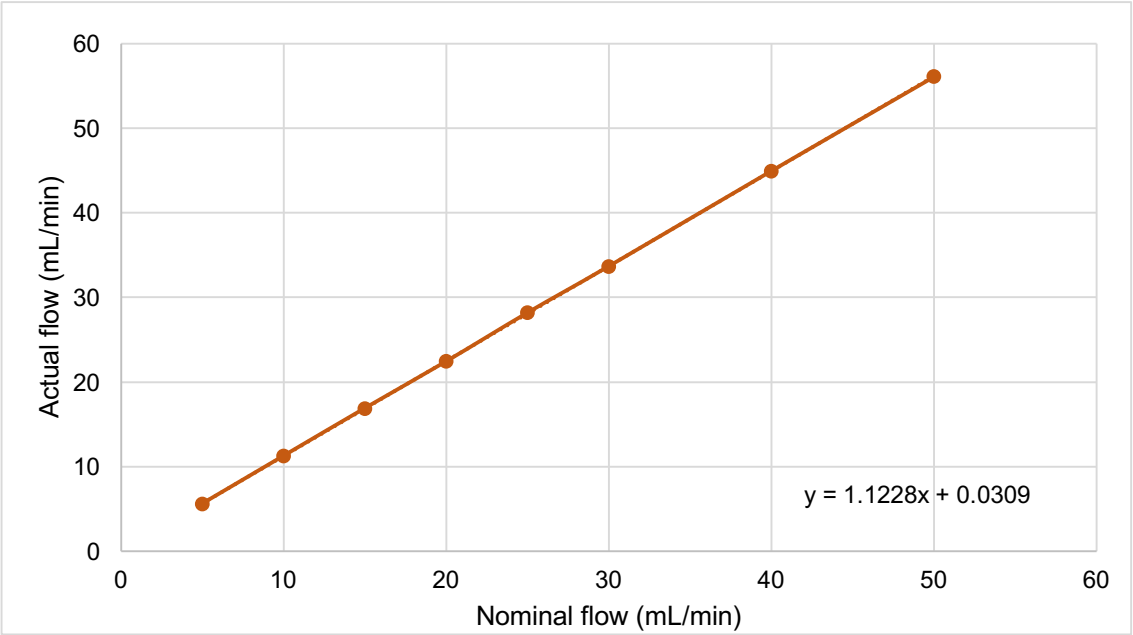

Figure 5. Experimentally-determined hydrogen MFC calibration curve

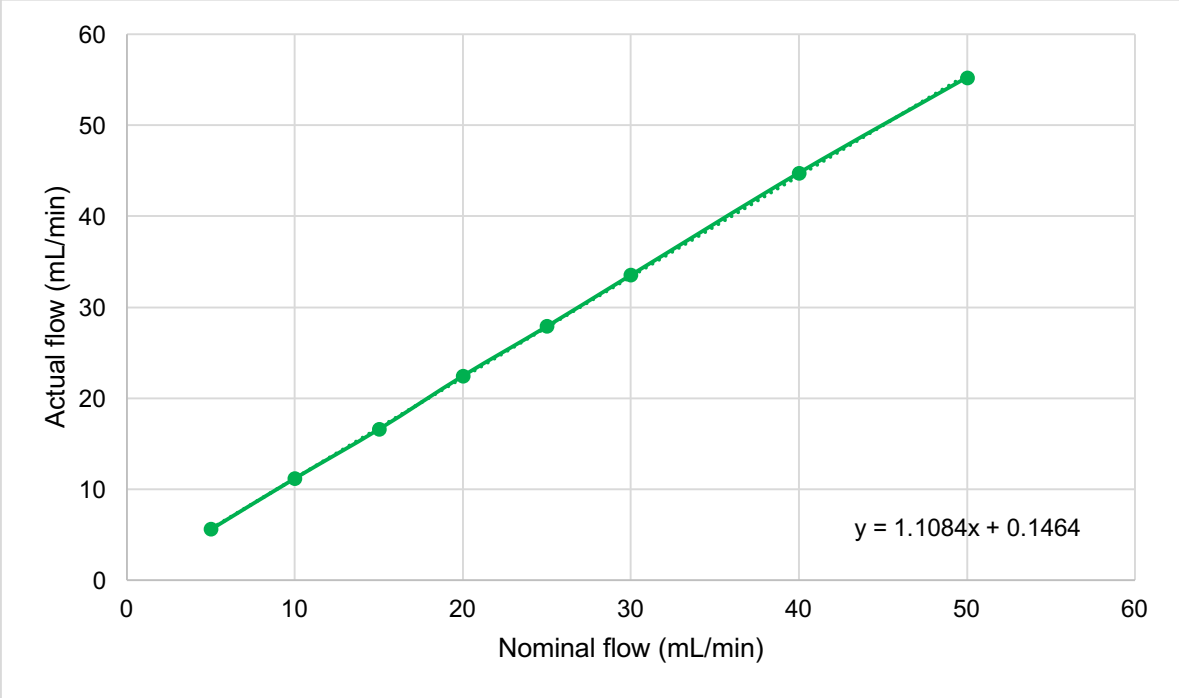

Figure 6. Experimentally-determined carbon monoxide MFC calibration curve

For the GC equipment calibration, a reactant gas mixture of Ar, H_2 and CO (1:6:3), representing the initial composition (100%) required for APFTS, was flowed into the GC *via* the sampling loop, using the previously calibrated MFCs, to obtain the reactant retention times and peak areas (H_2 and CO) relative to Ar. Following this, the percentage of the reactant gas mixture in the gas stream was decreased whilst keeping the Ar flow constant, to represent conversion of H_2 and CO at different percentages (85%, 75%, 60%, 50%, 35% and 25%). From the chromatograms, the areas of reactant gasses (H_2 and CO) relative to Ar were used to produce calibration curves as a function of conversion. From the calibration curves, for each area ratio of CO/Ar and H_2/Ar, the conversion fraction can be obtained. The calibration curves obtained can be observed in Figures 7 and 8:

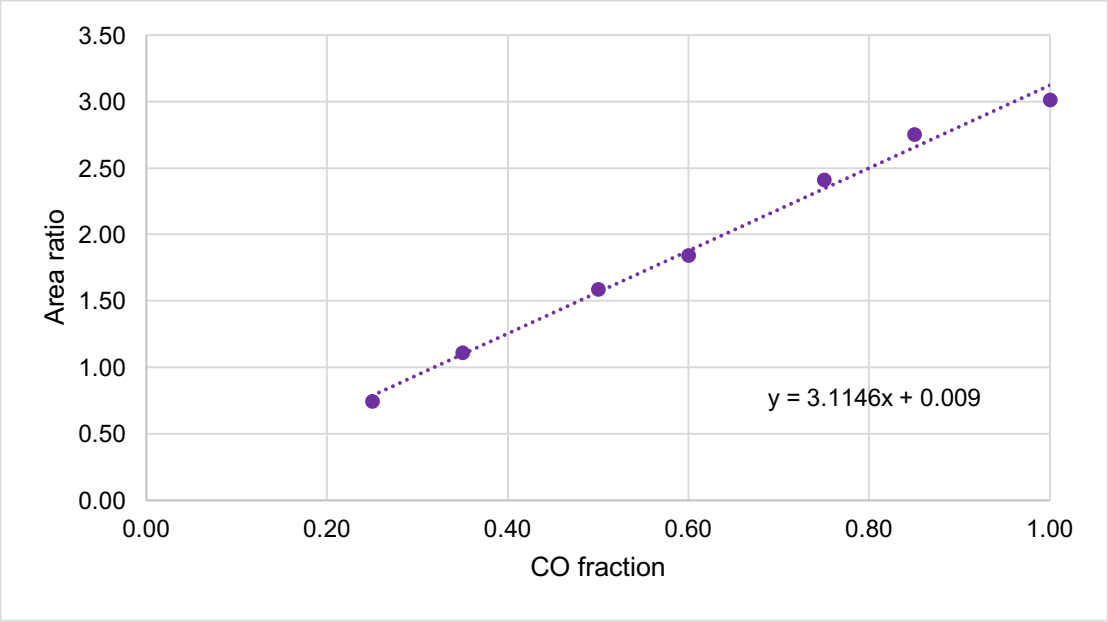

Figure 7. Experimentally-determined calibration curve used to calculate the CO fraction converted based on the area ratio of CO/Ar

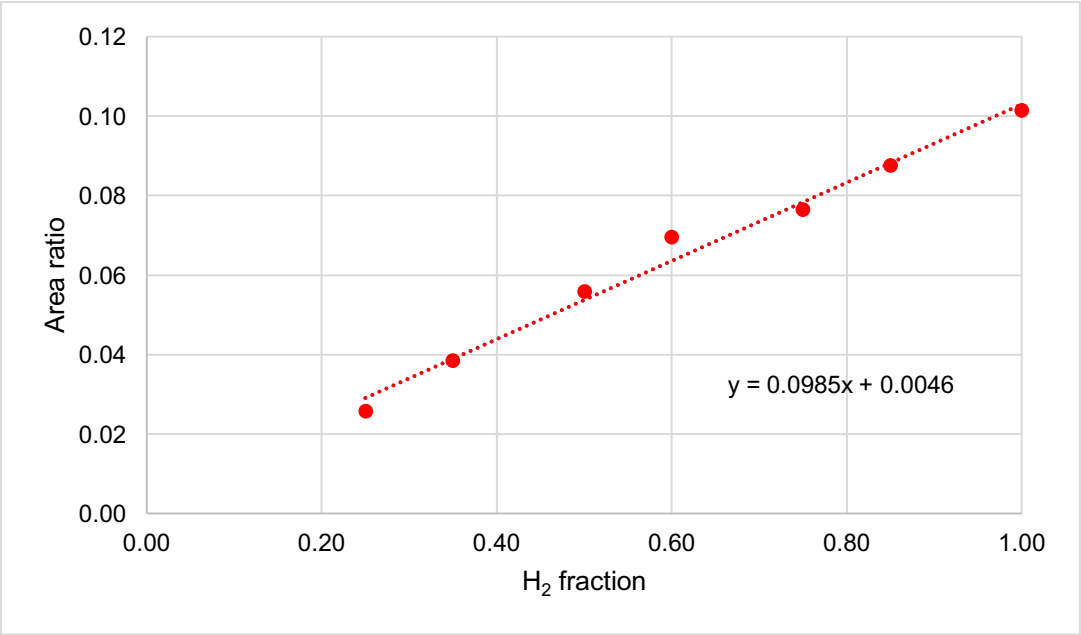

Figure 8. Experimentally-determined calibration curve to calculate the H_2 fraction converted based on the area ratio of H_2/Ar

To determine the catalytic activity calculation of each reaction, the following equation was used:[63]

Catalytic activity ($mol_{CO}\, mol^{-1}{}_{Co}\, h^{-1}$):

$$= \frac{\text{moles of CO consumed}}{(\text{moles of Co catalyst used})\ (\text{reaction time})}$$

3. Results and Discussion

With a view to understanding the role of water and support effects on Co/oxide-mediated APFTS, in particular the impact upon activity and selectivity of the reaction, catalytic experiments were conducted using Co-based catalysts in the low-temperature range of FTS (LTFT), *i.e.* at 190 °C. Each of the catalytic tests is described by the following stages:

1) Catalyst preparation by incipient wetness impregnation using SiO_2 or Al_2O_3 supports (see section 2.2).
2) Analysis of the oxide-bound cobalt content by ICP-OES (following exhaustive extraction of cobalt ions using concentrated nitric acid).
3) Catalytic testing conducted using a stainless steel reactor tube operating in batch mode as described in section 2.6.
4) Gas and liquid phase product analysis using gas chromatographic techniques.

3.1 Cobalt-based catalyst preparation

3.1.1 Incipient wetness impregnation

The cobalt catalysts were prepared *via* an incipient wetness impregnation method. Here, a known volume of an aqueous solution of $Co(NO_3)_2{\cdot}6H_2O$ was allowed to contact samples of both SiO_2 and Al_2O_3 support materials. Solution volumes were based on the pore volumes that had previously been experimentally determined by saturating the dried sample with water. Using this approach, as a result of capillary forces, the solution infiltrates into the pores of the supports giving dispersion of the cobalt precursor throughout the oxides.[18]

Initially, trial samples denoted as CP1-T (5% Co/SiO_2), CP2-T (5% Co/Al_2O_3) and CP3-T (10% Co/SiO_2) were prepared with the incipient wetness impregnation process being conducted in a round bottom flask, according to the methods described in sections 2.2.1 and 2.2.3. Here, the volume of water calculated for the impregnation (complete pore filling) based on the previously-determined oxide pore

volume was found to not be enough for the solution to be evenly distributed over the support, so additional water was added to ensure better impregnation of the sample. Then, for each sample, water was removed under reduced pressure on a rotary evaporator before thermal drying. However, due to the temperatures required to remove the water, cobalt-containing solution was also lost, which led to a lower than targeted Co concentration in the catalyst. Hence, to avoid Co loss, for subsequent samples, the rotary evaporator was no longer used before the sample drying step.

Without the rotational effect of the rotary evaporator, obtaining a uniform distribution of the Co precursor throughout the support during water removal was a concern for the subsequent catalyst samples. So, in order to optimize the catalyst preparation method, primarily to ensure a uniform distribution of the Co precursor throughout the oxide support, an alternative method was used to prepare samples with the same Co concentration as targetted for the earlier samples CP1-T, CP2-T, CP3-T, this time using a 10 mL plastic syringe (with the plunger removed) placed in a vertical position for the incipient wetness impregnation, as described in sections 2.2.2 and 2.2.4. The samples prepared using this modified approach are reported in Table 3, and are denoted as CP1 (5% Co/SiO_2), CP2 (5% Co/Al_2O_3) and CP3 (10% Co/SiO_2). Additional catalyst samples CP5 (10% Co/SiO_2), CP6 (10% Co/Al_2O_3), CP7 (10% Co/SiO_2), CP8 (10% Co/SiO_2) and CP9 (25% Co/SiO_2) were also prepared by the methods described in sections 2.2.2 and 2.2.4 using a 10 mL plastic syringe barrel for the incipient wetness impregnation. The catalyst samples CP1-CP9, as listed in Table 3, were the samples used for all cobalt loading analyses and catalytic tests.

Table 3. Summary of catalysts prepared *via* incipient wetness impregnation for APFTS testing

Sample name	Catalyst
CP1	5% Co/SiO_2
CP2	5% Co/Al_2O_3
CP3	10% Co/SiO_2
CP4	10% Co/SiO_2
CP5	10% Co/SiO_2
CP6	10% Co/Al_2O_3
CP7	10% Co/SiO_2
CP8	10% Co/SiO_2
CP9	25% Co/SiO_2

After incipient wetness impregnation, in each case a uniformly pink powder was obtained without the need for additional water. In no case was any liquid collected from the bottom of the syringe, indicating an optimum volume of water had been used, based on calculations from the experimentally-determined supports' pore volumes. To confirm a uniform distribution of the cobalt ions throughout the bulk of the oxide support material, an analysis of cobalt content was conducted, as described in section 3.1.2. Samples CP3, CP4, CP5, CP7 and CP8 have the same cobalt loading. These samples were prepared in order to probe and achieve reproducibility for the catalytic testing.

3.1.2 Cobalt loading analysis of impregnated oxide supports

3.1.2.1 Metal content analysis of samples CP1, CP2, CP3 and CP4

The metal content analysis for samples CP1 (5% Co/SiO_2), CP2 (5% Co/Al_2O_3), CP3 (10% Co/SiO_2) and CP4 (10% Co/SiO_2) was conducted as one batch according to the method described in section 2.3.1. The results of this analysis are reported in Table 4.

Table 4. Cobalt content/loading analysis determined experimentally by ICP-OES for catalysts CP1 (5% Co/SiO_2), CP2 (5% Co/Al_2O_3), CP3 (10% Co/SiO_2) and CP4 (10% Co/SiO_2); analysis of a control sample is included as a means of identifying any loss of cobalt through handling procedures

Catalyst	mg of Co present in the sample (experimental)
Control sample	4.57
	4.59
CP1 5% Co/SiO_2	3.50
	3.49
CP2 5% Co/Al_2O_3	3.71
	3.71
CP3 10% Co/SiO_2	4.09
	4.06
CP4 10% Co/SiO_2	4.08
	4.12

For each catalyst listed in Table 4, two samples were digested and submitted for ICP-OES analysis, with 5 mg of Co being expected to be present in each sample (theoretical). The experimental mass content for all of the catalysts is considerably

lower than the theoretical expected value. To explore the reason behind these low values of cobalt content measured, the acid digestion method was modified as described in section 2.3.2. The analysis results after this modification are described in section 3.1.2.2.

3.1.2.2 Metal content/loading analysis for samples CP3, CP4, CP5 and CP6

Samples CP3 (10% Co/SiO_2) and CP4 (10% Co/SiO_2) were analysed a second time along with samples CP5 (10% Co/SiO_2) and CP6 (10% Co/Al_2O_3). The metal content analysis was conducted according to the modified method described in section 2.3.2, with the experimental results of these analyses being reported in Table 5.

Table 5. Cobalt content analysis determined by ICP-OES for catalysts CP3 (10% Co/SiO_2), CP4 (10% Co/SiO_2) CP5 (10% Co/SiO_2) and CP6 (10% Co/Al_2O_3); analysis of a control sample is included as a means of identifying any loss of cobalt through handling procedures

Catalyst	mg of Co present in the sample (experimental)
Control sample	4.68
	4.72
CP3 10% Co/SiO_2	4.45
	4.60
CP4 10% Co/SiO_2	4.60
	4.68
CP5 10% Co/SiO_2	4.87
	5.00
CP6 10% Co/Al_2O_3	4.43
	4.47

Again, for each catalyst listed in Table 5, two samples were digested and submitted for ICP-OES analysis with 5 mg of Co being expected to be present in each sample (theoretical). The values of experimental mass content for all of the catalysts are higher than the values for the catalysts reported in Table 4 and are

essentially consistent across each material analysed. This suggests a better performance when using the modified method described in section 2.3.2.

3.1.2.3 Metal content/loading analysis of catalysts obtained using the optimized incipient wetness impregnation method described in sections 2.2.2 and 2.2.4

As described in section 3.1.1, an optimization of the incipient wetness impregnation method was explored using a plastic syringe barrel as a suitably-sized column to contain the oxide support. With the column clamped vertically, the oxide was treated dropwise with an aqueous solution of the cobalt-containing precursor. To determine the effectiveness of this revised method, a metal content/loading analysis by ICP-OES of a sample of 10%Co/SiO_2 catalyst (CP8, Table 3) prepared by this optimized incipient impregnation method was conducted. The results of this analysis are reported in Table 6.

Table 6. Metal content/loading analysis by ICP-OES to determine homogeneity of of 10%Co/SiO_2 catalyst prepared through slow drop-wise addition of an aqueous solution of $Co(NO_3)\cdot 6H_2O$, which was allowed to percolate through a packed column of the support held vertically (optimized method); analysis of a control sample is included as a means of identifying any loss of cobalt through handling procedures

Catalyst	**Syringe section**	**mg of Co present in the sample (experimental)**
Control sample		4.66
		4.74
CP8 10% Co/SiO_2	1	1.77
		1.80
	2	1.74
		1.74
	3	1.82
		1.86
	4	1.65
		1.70
	5	1.70
		1.71

Samples of the resulting impregnated material were carefully removed from the plastic syringe to allow ICP-OES analysis of portions of the material along the length of the oxide bed (syringe sections 1-5). The syringe section 1 represents a sample taken from the highest section of the plastic syringe with the impregnated catalyst. The syringe section 5 represents a sample taken from the bottom of the plastic syringe. For each sample of catalyst removed from the syringe section

analyzed, two samples were digested and submitted for ICP-OES analysis, with 5 mg of Co being expected to be present in each sample (theoretical loading). Consistent values of metal content were obtained for samples taken from the different sections of the plastic syringe with the impregnated catalyst. The lowest metal content value was 1.65 mg of Co, reported for sample 1 of syringe section 4. The highest metal content was 1.86 mg of Co, reported for sample 2 of syringe section 3. This small variation in determined metal content indicates a good distribution of the metal precursor throughout the support by the incipient impregnation method employed (sections sections 2.2.2 and 2.2.4). However, these experimental values are significantly lower than those expected from the theoretical metal content values (less than 50% mass). This difference in loading is attributed to the fact that after the incipient wetness impregnation, the samples were not dried, so the water content affected the weight of the sample used for ICP-OES sample preparation.

To further explore how sample preparation affects the analysis of the cobalt loading by ICP-OES, another batch of samples was analyzed, but for these analyses after the incipient wetness impregnation each sample was placed into a small vial and dried in a oven for 12 h at 110 °C before being subject to treatment with *aqua regia*. The experimental metal content values expected for different impregnated zones of this batch of 10% Co/SiO_2 (sample CP8 from Table 3) are reported in Table 7.

Table 7. Metal content/loading analysis as determined by ICP-OES to determine homogeneity of 10%Co/SiO_2 catalyst sample prepared using the optimized method after being dried for 12 h at 110 °C; analysis of a control sample is included as a means of identifying any loss of cobalt through handling procedures

Catalyst	**Syringe Section***	**mg of Co present in the simple (experimental)**
Control sample		4.64
		4.58
CP8 10% Co/SiO_2	1	4.63
		4.69
	2	4.61
		4.66
	3	4.12
		4.22
	4	4.38
		4.39

* See experimental sections 2.2.2 and 2.2.4 for further details, 1 being the top of the column and 4 the bottom

After the batch of samples of a 10% Co/SiO_2 catalyst (CP8) described in Table 7 were dried for 12 h at 110 °C after incipient wetness impregnation, four samples of the resulting impregnated material were carefully removed from the plastic syringe barrel to allow ICP-OES analysis of portions of the material along the length of the bed (syringe sections 1-4). The syringe section 1 represents a sample taken from the highest section of the plastic syringe with the impregnated catalyst. The syringe section 4 represents a sample taken from the bottom of the plastic syringe. For

each sample of catalyst removed from the syringe section analyzed, two samples were digested and submitted for ICP-OES analysis and 5 mg of Co were expected to be present in each sample (theoretical). Consistent values of metal content were obtained for samples taken from different sections of the plastic syringe with the impregnated catalyst, indicating eveness of the impregnation method. The lowest metal content value was 4.12 mg of Co, reported for sample 1 of syringe section 3. The highest metal content value was 4.69 mg of Co, reported for sample 2 of syringe section 1. This small variation in metal content values indicates a good distribution of the metal precursor on the support by the incipient impregnation method employed (sections 2.2.2 and 2.2.4).

3.1.3 TEM Analysis of Cobalt/oxide catalysts CP1, CP2, CP3, CP5 and CP6

Samples 5% Co/SiO_2 (CP1), 5% Co/Al_2O_3 (CP2), 10% Co/SiO_2 (CP3, CP5) and 10% Co/Al_2O_3 (CP6) (see Table 3) were analysed by transmission electron microscopy (TEM). This characterization was conducted after the catalyst samples were reduced *ex situ* at 350 °C for 12 h under an H_2/N_2 atmosphere (50% vol.of H_2 in N_2). The images for these catalyst samples are reported in Figures 9, 10, 11, 12, and 13.

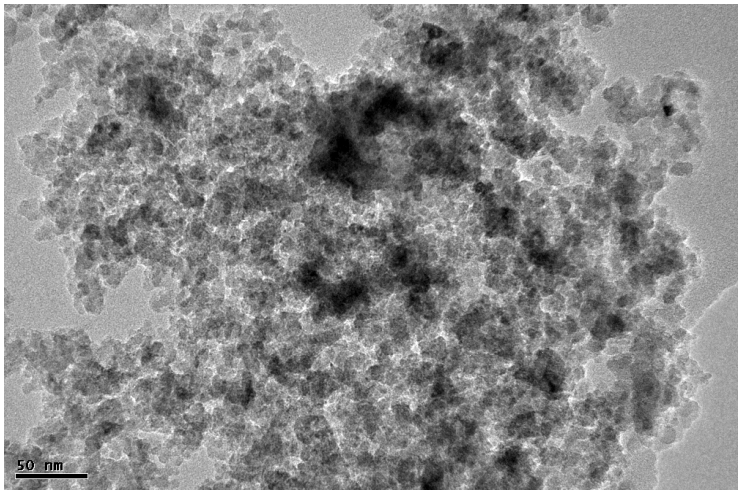

Figure 9. TEM image of sample CP1 (5% Co/SiO_2 catalyst)

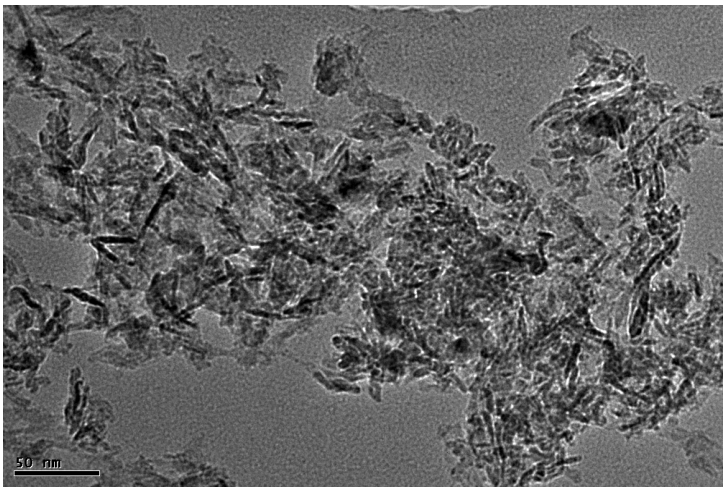

Figure 10. TEM image of sample CP2 (5% Co/Al_2O_3 catalyst)

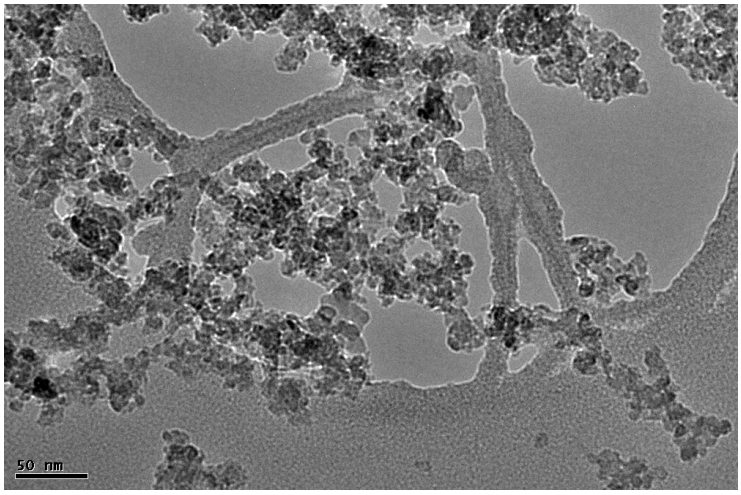

Figure 11. TEM image of sample CP3 (10% Co/SiO_2 catalyst)

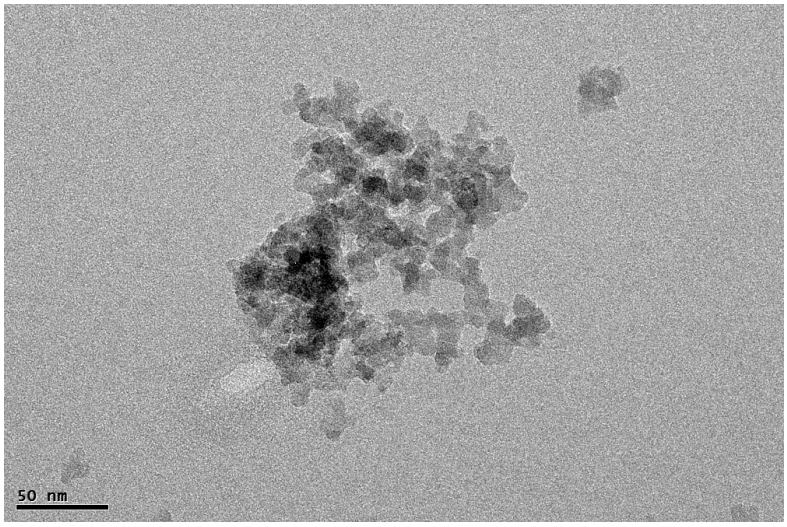

Figure 12. TEM image of sample CP5 (10% Co/SiO_2 catalyst)

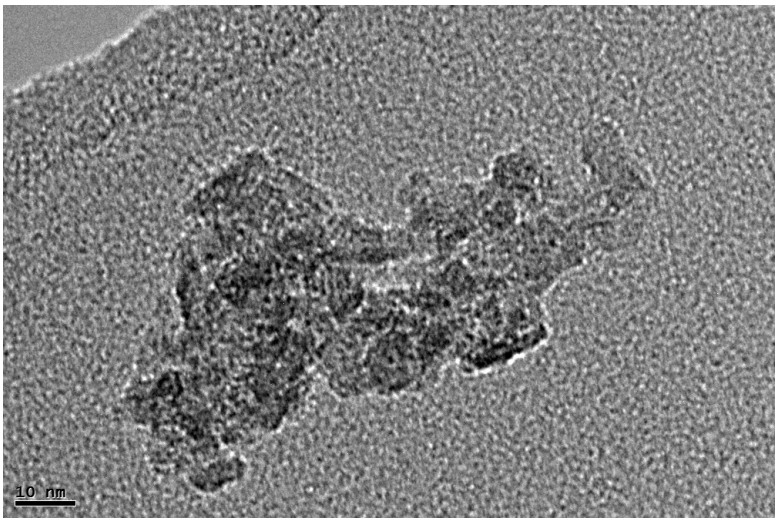

Figure 13. TEM image of sample CP6 (10% Co/Al_2O_3 catalyst)

A significant aggregation of cobalt particles was observed from the TEM images for all of the catalyst samples analyzed. Because of the irregular structure, *i.e.* flocculent structure, formed from particles agglomerating to large particle clumps, it was not possible to analyze the size distribution of the cobalt particles. Individual particles were not identified from the agglomerated particles, restricting the size distribution analysis. Dark sections in the particle clusters were observed for all of the catalyst samples, which represent Co containing regions, as confirmed by the energy dispersive X-ray (EDX) capability of the microscope. In Figures 10 and 13, a more elongated shape of the particle clusters was observed for the Al_2O_3 supported samples, compared to the SiO_2 samples; the origins of this difference remain unclear.

3.2 Catalytic performance of Co-based supported catalysts

3.2.1 Catalytic testing using 5% Co/SiO_2, 5% Co/Al_2O_3 and 10% Co/SiO_2 catalysts reduced *in situ*

The catalytic testing of the different Co-based supported catalysts prepared was conducted according to the method described in section 2.6. Here, gas chromatographic techniques were used to probe reactions, with analysis being undertaken at the end of each individual catalytic run. Following initial catalyst preparation *via* incipient wetness impregnation of the relevant oxide support (SiO_2 or Al_2O_3), subsequently each material was subject to *ex situ* drying and calcination processes (see Sections 2.2.2 and 2.2.4). This latter steps resulted in the colour of the impregnated samples shifting from pink to black. The "activated" black material was used as a catalyst for the APFTS reaction by being transferred into the reactor vessel and subsequently mixed with water for APFTS. The catalytic testing for APFTS was conducted according to the parameters described in section 2.2 using the materials CP1 (5% Co/SiO_2), CP2 (5% Co/Al_2O_3), CP3 (10% Co/SiO_2), and CP4 (10% Co/SiO_2) (see Table 3). The testing was performed with no stirring and using 17 mg of catalyst suspended in water (5 ml). After 48 h, GC analysis of the head space volatile components (as described on section 2.3.1) showed that no observable new gaseous products had been produced. Only the reactant gasses H_2, CO, and Ar were observed.

It was envisaged that under the reaction conditions employed, the relative concentration of the desired alkane products would be quite low. Consequently, in order to assess whether these catalysts were indeed active, subsequent reactions were attempted with higher catalyst loadings, namely using 200 mg of catalyst. Additionally, in order to facilitate reaction by enhancing reactant gas diffusion through the water, reaction stirring was introduced addition of a raised disc Teflon-coated magnetic stirrer bar and placing the reactor tube on top of a magnetic stirrer plate. Subsequent catalytic testing for APFTS was conducted according to the parameters described on section 2.2 using the catalyst samples CP1 (5% Co/SiO_2), CP2 (5% Co/Al_2O_3), CP3 (10% Co/SiO_2), and CP4 (10% Co/SiO_2) (see

Table 3). Again, at the end of the reaction GC chromatographic analysis of the volatile head space gases detected no new products, with only the reactant gasses H_2, CO and Ar being detected.

3.2.2 Catalytic testing using 5% Co/SiO_2, 5% Co/Al_2O_3, 10% Co/SiO_2, 10% Co/Al_2O_3 and 25% Co/SiO_2 catalysts reduced *ex situ*

Since the catalytic tests described in section 3.2.1 were unsuccessful, focus was placed on the catalyst preparation method with a view to probing whether this may be the cause of the lack of reactivity. After the incipient wetness impregnation optimization reported on section 3.1 using a plastic syringe barrel to contain the support material had been explored and found to provide a satisfactory route to a well-dispersed cobalt precursor on the oxide supports, the next main concern was the necessary catalyst reduction step to obtain active sites that would promote the reaction. For the catalytic tests described above, the reduction of the catalyst had been made *in situ* (in the reaction vessel immediately prior to addition of reactant gases and after being mixed with water) at 150 °C for 2 h and 14 bar of H_2 as described in section 2.6. With a view to ensuring a more rigorous and effective reduction of the catalyst, an alternative *ex situ* reduction step (see section 2.5) was then explored as suggested previously in the literature.[53] To this end, the catalyst samples prepared *via* the incipient wetness impregnation method discussed above were reduced *ex situ* at 350 °C for 12 h under a H_2/N_2 atmosphere (50% vol. of H_2 in N_2). These catalyst samples were then quickly transferred into the reactor tube (exposed to the laboratory atmosphere) mixed with water and then subject to a further *in situ* treatment with H_2 at 14 bar, 150 °C for 2 h. The APFTS catalytic testing results for these samples reduced with the extra *ex situ* step before the "*in situ*" reduction are reported in Table 8.

Table 8. APFTS catalytic testing conducted at 190 °C and 20 bar, over 48 h reaction time, for different Co-based supported catalysts after reduction *ex-situ* of the catalysts including gaseous products observed by GC

Run	Temperature (°C)	Initial pressure (bar)	Final pressure (bar)	Catalyst name	[Co]	Catalyst Support	Volume of H_2O (ml)	Products observed
1	190	21.08	NR	CP1	5%	SiO_2	5	methane
2	190	20.79	14.75	CP2	5%	Al_2O_3	5	methane, ethylene, ethane, carbon dioxide
3	190	20.74	20.65	CP3	10%	SiO_2	5	methane
4	190	20.89	20.89	CP4	10%	SiO_2	5	methane
5	190	20.70	NR	CP5	10%	SiO_2	5	methane, ethylene, ethane
6	190	21.03	20.03	CP6	10%	Al_2O_3	5	methane, ethylene, ethane, carbon dioxide
7	190	20.79	NR	CP7	10%	SiO_2	5	methane, ethylene, ethane
8	190	20.74	20.13	CP7	10%	SiO_2	5	methane, ethylene, ethane
9	220	20.51	20.51	CP8	10%	SiO_2	5	methane, ethylene, ethane
10	190	20.93	19.98	CP9	25%	SiO_2	5	Methane, ethylene, ethane

NR* = None recorded

The catalyst names are indicated in accordance with information given in Table 3.

After reducing *ex situ* the 5%Co/SiO_2 catalyst (sample CP1 from Table 3) and conducting the catalytic testing, a signal corresponding to methane (CH_4) was observed, in addition to those from the reactant gases, in the gas chromatogram from the head space gas product analysis undertaken. Retention times were

attributed by comparison with GC analysis of authentic samples of each gas. In contrast, post-reaction gas analysis for the 5%Co/Al_2O_3 catalyst (CP2, Table 3) test revealed the presence of signals from methane, ethylene (C_2H_4), ethane (C_2H_6), and carbon dioxide (CO_2). For both the tests carried out with CP1 and CP2 the observation of these products is consistent with these catalysts (activated as described) being active for APFTS under the reaction conditions described.

It should be noted that, despite observation of new gaseous products, the pressure difference measured between the start and end of the catalytic test was found to be negligible, which suggests a low catalytic activity. However, there was indication of catalytic activity based on the products observed for all of the runs performed after the optimization of the reduction step. For runs 1,5 and 7 (Table 8), the final pressures after catalytic testing were not recorded due to omission of the observer.

Methane, ethylene, ethane and carbon dioxide were the only gas products observed by gas chromatography for APFTS. It must be noted that the area peaks observed for ethylene and ethane were much lower, compared to the peak corresponding to methane. Carbon dioxide was only obtained using Al_2O_3 as a support for the catalyst. It was not detected when using SiO_2 as a support. For comparison of the selectivities, based on the products observed in the set of experiments described in Table 8, the closest comparable Al_2O_3-supported Co-based catalyst system described in the literature is that described by Pendyala *et al*. using a 0.5%Pt-25%Co/Al_2O_3 catalyst for APFTS.[63] In their report, Pendyala and coworkers reported hydrocarbons as the predominant products (67%), oxygenate selectivity of 11% and the remaining being carbon dioxide (22%). The authors conducted APFTS at 3 MPa and 165 °C for 24 h in a 1 L stainless steel autoclave in the batch mode operation. Pendyala and coworkers concluded that the selectivity towards carbon dioxide suggests that at least a part of the cobalt had been oxidized to an oxide phase that is active for the water-gas shift, which can also be the case of the Al_2O_3-supported catalysts as reported in Table 8, since the

same temperature (350 °C) was used to externally reduced the catalysts. Pendyala and coworkers also reported a selectivity towards methane of 18%, which was higher than the selectivity (7%) reported for both unsupported and zeolite supported ruthenium catalysts also used for APFTS in their report. The results of Pendyala and coworkers and those presented in Table 8 suggest that using an oxide support results in methane formation for APFTS to a higher extent than Ru-based systems.

Ethylene and ethane were not observed in runs 1, 3 and 4, which correspond to catalysts using SiO_2 as a support. Runs 5, 7 and 8 were conducted at the same temperature (190 °C) and using a 10%Co/SiO_2 catalyst, showing consistence in the formation of methane, ethylene and ethane as products. Run 9 was conducted at a higher temperature of 220 °C and run 10 was conducted using a 25%Co/SiO_2 catalyst and both runs showed the same consistency in the products obtained as runs 5, 7 and 8.

3.2.3 Conversion percentages for 5% Co/SiO_2, 5% Co/Al_2O_3, 10% Co/SiO_2, 10% Co/Al_2O_3 and 25% Co/SiO_2 catalysts reduced *ex situ* using calibration curves

The percentage conversion for H_2 and CO calculated by calibration curves were determined (see section 2.8). The percentage conversions were calculated based on the area ratios of H_2 and CO relative to Ar obtained from the peak integration of the GC chromatograms and are recorded for the different catalytic testing runs in Table 9.

Table 9. APFTS catalytic activity calculated directly from GC calibration curves.

Run	Temperature (°C)	Catalyst name	[Co]	Catalyst Support	H_2 conversion (%)	CO conversion (%)
1	190	CP1	5%	SiO_2	168	113
2	190	CP2	5%	Al_2O_3	52	41
3	190	CP3	10%	SiO_2	53	45
4	190	CP4	10%	SiO_2	41	35
5	190	CP5	10%	SiO_2	ND	ND
6	190	CP6	10%	Al_2O_3	42	38
7	190	CP7	10%	SiO_2	52	38
8	190	CP7	10%	SiO_2	48	43
9	220	CP8	10%	SiO_2	52	49
10	190	CP9	25%	SiO_2	207	38

The percentage conversions obtained though analysis of the head space gases at the end of each catalytic run using separate GC calibration curves (Table 9) are clearly incorrect and do not show a correlation with the extremely small differences in pressure measure for each catalytic test *(i.e.* pressure difference measured over the reaction time) reported in Table 8. It is proposed that the variation in the values of conversion obtained using this approach suffer significantly as a result of

variations in flow rates of the gas samples from the reactor into the GC, as well as the actual conversions being extremely small and hence neglible compared with the calibrations. Consequently, an alternative approach was explored for the determination of APFTS catalytic activities for the tests undertaken here.

3.2.4 Catalytic activity calculations for APFTS using for 5% Co/SiO_2, 5% Co/Al_2O_3, 10% Co/SiO_2, 10% Co/Al_2O_3 and 25% Co/SiO_2 catalysts reduced *ex situ* based on methane area peaks

In order to provide an estimate of the activity of each of the catalysts a different approach was explored. Since the formation of methane was observed to occur under the reaction conditions employed (Table 8), signifying some (limited) FT reaction, an estimate of catalytic activity for one of the more active catalysts was made on the basis of the GC FID signal for methane. To achieve this, a calibration of the gas chromatograph for methane was conducted using two commercial gas mixtures provided by Calgaz Ltd. The first gas mixture contained 1% (vol.) methane, 1% ethane, 1% propane, 1% n-butane, 1% n-pentane with an N_2 balance. The second gas mixture contained 2% (vol.) of methane, 4% carbon monoxide, 15% carbon dioxide, 20% hydrogen with a N_2 balance. Each gas mixture was flowed into the gas chromatography equipment according to the method described in section 2.7.1, although due to the gas volumes and pressures associated with these calibration samples, it was impractical to use a gas flow meter. For the gas mixture containing 1% (vol.) of methane, a peak of the corresponding gas was observed, with an area of 3135 μV·min for one experimental run. For the gas mixture containing 2 % (vol.) of methane, two experimental runs averaged an area of 15289 μV·min for the corresponding methane peaks. This last value was divided by a factor of two, so to obtain the area corresponding to an equivalent gas mixture of 1% (vol.) of methane, resulting in a value of 7644 μV·min. A significant difference in the calculated area values for each gas mixture at 1% (vol.) of methane was observed. This difference in values is attributed to the fact that the gas mixtures were flowed into the GC inlet sampling loop at a different rate, since the flow meter was not used. An average peak area

of 5390 μV·min for methane was used for further calculations, calculated by the average in peak area values for methane at 1% (vol.) in each gas mixture:

Methane peak area for gas mixture containing 1% (vol.) of methane = **3135 μV·min**

Averaged methane peak area for gas mixture containing 2% (vol.) of methane = **15289 μV·min**

Average peak area of methane at 1% (vol.) used for further calculations:

$$= \frac{3135 + 7644}{2} = \mathbf{5390\ \mu V.Min}$$

The area obtained from the previously-described methane calibration at 1% (vol.) was used to calculate the volume percentage of methane present in the gas product mixtures to very roughly estimate the relative activity of the variously-prepared catalysts (See Table 8). The calculations will be exemplified using the area value of methane obtained after catalytic testing for a 10%Co/Al_2O_3 catalyst (sample CP6 from Table 3). The reported area for when using this sample was 559 μV.Min. Using the methane calibration, this value represents a 0.10 % (vol.) of methane present in the gas product mixture:

Average peak area of methane at 1% (vol.) = **5390 µV.Min**

Peak area of methane for a 10%Co/Al_2O_3 catalyst (sample CP6 from Table 3) = **559 µV.Min**

Methane percentage (vol.) in gas product mixture for a 10%Co/Al_2O_3 catalyst (sample CP6 from Table 3):

$$= \frac{(\text{peak area of methane for CP6})(0.01)}{\text{average peak area of methane at 1\% vol.}} = \frac{(559)(0.01)}{5390} * 100 = \mathbf{0.1}\ \%\ (\mathbf{vol.})$$

The volume percentage of methane multiplied by the volume of the reactor tube represented the volume of carbon monoxide converted for each catalytic testing run. The reactor volume was assumed to be 15 mL, which is the volume corresponding to the reactor tube, although it must be noted that the total volume of the reactor system is bigger than 15 mL, since the pressure of the gasses in the reactor system were distributed not just along the reactor tube, but along the tubing sections described in section 2.6 as well – so this is a source of error. For the 10%Co/Al_2O_3 catalyst (sample CP6 from Table 3), the 0.10% (vol.) of methane present in the gas product mixture (or 0.001 represented as a decimal value) was multiplied by the reactor tube volume, resulting in a volume of carbon monoxide converted of 1.5 ×10^{-8} m^3.

Volume of reactor tube in m^3 = **1.5×10^{-5} m^3**

Volume of carbon monoxide converted:

$$= (1.5\times10^{-5})(0.001) = \mathbf{1.5\times10^{-8}}\ \boldsymbol{m^3}$$

With the values of carbon monoxide volume converted, the moles of carbon monoxide converted during catalytic testing were calculated using the ideal gas law equation shown in Figure 14.

$$PV = nRT$$

Figure 14. Ideal gas law equation

A gas constant value of R = 8.314 m^3 Pa K^{-1} mol^{-1} was used for calculations. The pressure (P) represented the total pressure obtained by the pressurization of Ar, H_2 and CO before catalytic testing for each experimental run. A room temperature value T = 298 K was assumed. The moles of CO converted for the 10%Co/Al_2O_3 catalyst (sample CP6 from Table 3) were 1.3 ×10^{-5} moles of CO:

Moles of CO converted:

$$\mathrm{n} = \frac{\mathrm{PV}}{\mathrm{RT}} = \frac{(2103000\ \mathrm{Pa}\ )(1.5\times10^{-8}\mathrm{m}^3)}{(8.314\ \mathrm{m}^3\mathrm{PaK}^{-1}\mathrm{mol}^{-1})(298\ \mathrm{K})} = \mathbf{1.3\times10^{-5}\ mol}$$

Subsequently, the moles of Co used for catalytic testing were calculated based on the known mass of catalyst sample used for each catalytic run and the experimental mass percentage of Co present for each sample. By way of example, for the catalytic testing using the 10% Co/Al_2O_3 catalyst (sample CP6 from Table 3; Run 6 Table 10), 181.1 mg of catalyst were used, corresponding to 0.255 ×10^{-3} moles of cobalt.

Finally, the catalytic activity was calculated according to the equation shown in section 2.8. All of the catalytic testing runs were conducted over a 48 h reaction time. The catalytic activity results for APFTS using different Co-based supported catalysts are presented on Table 10. It should be noted that the errors for the catalytic activity values described here (Table 10) are large due to the number of assumptions made for the calculations (described above) and the accuracy of the methane GC calibrations achievable in the timeframe of this project. The catalytic activity reported when using a 10% Co/Al_2O_3 catalyst (sample CP6 Table 3; Run 6 Table 10) was 1×10^{-3} mol_{CO} $mol^{-1}{}_{Co}$ h^{-1}. The activities for Runs 1-5, 7-10 described in Table 10 were determined in the same manner.

Catalytic activity (mol_{CO} $mol^{-1}{}_{Co}$ h^{-1}) for 10% Co/Al_2O_3 catalyst (sample CP6 Table 3; Run 6 Table 10):

$$= \frac{\text{moles of CO consumed}}{(\text{moles of Co catalyst used})\ (\text{reaction time})} = \frac{1.3\times10^{-5} mol_{co}}{(0.255\times10^{-3} mol_{Co})(48\ h)}$$

$$= \mathbf{1\times10^{-3}}\ \boldsymbol{mol_{CO} mol_{Co}{}^{-1} h^{-1}}$$

Table 10. Catalytic activity for APFTS conducted at 190 °C and 20 bar, over 48 h reaction time using Co-based supported catalysts based on methane production and calculations using gas mixtures for methane calibration.

Run	Catalyst name	[Co]	Catalyst Support	Catalytic activity ($mol_{CO}\ mol^{-1}_{Co}\ h^{-1}$)
1	CP1	5%	SiO_2	2.4×10^{-6}
2	CP2	5%	Al_2O_3	3.9×10^{-4}
3	CP3	10%	SiO_2	1.3×10^{-5}
4	CP4	10%	SiO_2	1.4×10^{-4}
5	CP5	10%	SiO_2	7×10^{-4}
6	CP6	10%	Al_2O_3	1×10^{-3}
7	CP7	10%	SiO_2	5×10^{-4}
8	CP7	10%	SiO_2	2.2×10^{-4}
9	CP8	10%	SiO_2	2.3×10^{-4}
10	CP9	25%	SiO_2	9.3×10^{-4}

* The catalytic activity for runs 1,2,7,8 and 10 were calculated based on the theoretical mass percentage of Co present in each catalyst sample

To provide a comparison of the activities determined in the set of experiments described in Table 10, the closest comparable Al_2O_3-supported Co-based catalyst system described in the literatura was used, namely that described by Pendyala *et al*.[63] However, it cannot be regarded as a perfect system for comparison, since the catalyst incorporated a Pt promotor, something that can significantly alter activity.[64] This aside, this system reported Pendyala and coworkers gave a catalytic activity of 0.2455 $mol_{CO}\ mol^{-1}_{Co}\ h^{-1}$ for APFTS at 165 °C and 3 MPa using a 0.5%Pt-25%Co/Al_2O_3 catalyst.[1] This catalytic activity reported by Pendyala is higher by three orders of magnitude compared to the catalytic activity obtained as a part of the present work for a 10% Co/Al_2O_3 catalyst, but as will be discussed below there will be a significant Pt promotion effect. An alternative comparison may be made

with the system reported by Wang *et al*. based on a Co nanoparticle catalyst prepared by reduction of an appropriate precursor using $NaBH_4$, which gave a catalytic activity of 0.09 mol_{CO} mol^{-1}_{Co} h^{-1}.[62] This catalytic activity reported by Wang *et al*. represents the activity of a Co catalyst without the influence of an oxide support. Evidently, there is a significant difference in the catalytic activity results between those reported in the present work and those reported in literature for Co-based catalysts. However, there are significant differences in the methodologies employed and the nature of the catalysts themselves, factors that will be further discussed below.

The 0.5%Pt-25%Co/Al_2O_3 catalyst used by Pendyala *et al*. for AFPTS was prepared by a slurry impregnation method, and cobalt nitrate was used as a precursor. For their slurry impregnation, Pendyala *et al*. used a volume of cobalt precursor solution approximately 2.5 times the pore volume of the catalyst. For the catalysts prepared in the present thesis (as described in section 2.2), the same volume of cobalt precursor solution as that of the pore volume of the oxide supports was used.

Notably, Pendyala *et al*. used a metal content of 25% of Co by weight in the catalyst. This metal content percentage is 2.5 higher than the theoretical metal content of the catalysts reported here. To achieve such a metal content, Pendyala *et al*. conducted two impregnation steps, each to load 12.5 % of Co by weight. Between each step, the catalyst was dried under vacuum using a rotary evaporator at 80 °C, and the temperature was slowly increased to 100 °C. After the second impregnation/drying step, the catalyst was calcined under an air flow at 350 °C, which corresponds to the same calcination temperature used for the catalysts prepared in the present work. The effect of the metal loading for a Co-based supported catalyst used for APFTS represent a subject of interest, such as the effect of using different oxide supports.

The final, but perhaps the most significant difference between the catalyst prepared by Pendyala *et al*. and the catalysts prepared in this thesis, is Pendyala's use of a Pt promoter. As described in section 1.5.1.3, it has been established that promoters have a strong impact on the structure and dispersion of Co species, FTS reaction rates, and selectivities. However, the impact of the promoter here is hard to establish since in their report, Pendyala *et al*. only compared the catalytic activity of their 0.5%Pt-25%Co/Al_2O_3 catalyst to that of a Ru nanoparticle system and a catalyst in which Ru was supported on zeolite-Y. This analysis revealed that the Co/Pt system's activity was the lowest.

A comparison, however, may be made between the Co-NP system reported by Wang *et al*. and the Pt-promoted, oxide-supported system used by Pendyala *et al*. The catalytic activity of the 0.5%Pt-25%Co/Al_2O_3 catalyst reported by Pendyala *et al*. (0.2455 mol_{CO} mol^{-1}_{Co} h^{-1}) is higher than the activity reported by Wang *et al*. for their unsupported Co nanoparticle catalyst system (0.09 mol_{CO} mol^{-1}_{Co} h^{-1}). This is consistent with the observation made by Wang and co-workers who also observed an increase in catalytic activity to 0.6 mol_{CO} mol^{-1}_{Co} h^{-1} following addition of a small amount of Pt (molar ratio of Pt:Co = 0.05).[62] This value of catalytic activity for the promoted system is around one order of magnitude higher than that of the pure Co catalyst, and also higher than that reported by Pendyala *et al*. (0.5%Pt-25%Co/Al_2O_3). As anticipated, these studies indicate that the effect of promoters for APFTS when using supported and unsupported catalysts can have a very significant effect.

With a view to eliminating any effects that may cause the catalysts for APFTS reported in this present work (Section 2.6) using a batch-operating mode reactor system to be lower than expected, the volume of reactant gasses (Ar, H_2 and CO) in contact with the catalyst in suspension in the water may be an area for further investigation. The reactant gasses enter the reactor *via* the input needle valve, which is located at the top of the reactor system. Consequently, it may be

envisaged that the gas mixing with the suspension of the catalyst in water located at the bottom of the reactor tube may have been poor. It can be possible that during the catalytic reaction, only a small volume of reactant gasses are in contact with the catalyst in the reaction zone, hence significantly impacting on the system's activity. Indeed, to get round such problems, one possibility when using a batch-operating mode reactor for APFTS is to use a nanoparticle catalyst soluble in the water phase, rather than a catalyst present as suspension. This was suggested by Chao-Xian *et al*., who achieved a high catalytic activity of 6.9 $mol_{CO}mol_{Ru}^{-1}h^{-1}$ using water-soluble Ru nanoclusters stabilized by poly(*N*-vinyl-2-pyrrolidone) (PVP) for APFTS.[7] Furthermore, Lingtao *et al*.[61] have conducted APFTS using a continuous flow reactor where the syngas can be fed into the reactor continuously, while the product mixture is withdrawn from the reactor then separated from the catalyst. The use of a continuous flow reactor is a crucial step for the feasibility demonstration for the future industrial application of APFTS. In their report, Lingtao *et al*. used Ru nanoparticles reduced by hydrogen in the presence of PVP, with the resulting catalyst showing a high catalytic activity of 6.9 $mol_{CO}\ mol_{Ru}^{-1}\ h^{-1}$. Based on these studies, it is clear that the reactor design can be crucial for good catalytic performance in APFTS systems.

3.2.5 Liquid product analysis of products obtained from catalytic testing (run 1 from Table 8) of a 5% Co/SiO_2 catalyst (CP1)

The liquid phase obtained after catalytic testing of sample CP1 (5% Co/SiO_2, Table 3) was used for liquid products analysis. After APFTS, the reactor tube was detached from the gland fitting. The liquid phase (a black liquid) from the reactor vessel was poured into a small glass vial. After centrifugation, the liquid phase obtained was extracted using diethyl ether. No signals other than those for diethyl ether were observed by gas chromatography. Since only a very small pressure change was observed over the catalytic test duration, which is indicative of very low catalytic activity, hence it is reasonable to suggest that the formation of longer hydrocarbon chain liquid products was not likely to occur, consistent with this analysis.

4. Conclusions

In exploring the chemistry of APFTS using a cobalt-only supported catalyst, this project focused on the impact of the different stages that constitute the catalytic process. In particular the effects of the catalyst preparation using an incipient wetness impregnation method, the analysis of the oxide-bound cobalt content by ICP-OES, the catalytic testing operating in batch mode, and the gas and liquid phase products analysis were investigated.

The 5% Co/SiO_2, 5% Co/Al_2O_3, 10%Co/SiO_2 and 25% Co/SiO_2 catalyst samples were prepared *via* incipient wetness impregnation. Establishing a uniform dispersion of the Co precursor solution across the surface and within the pores of the oxide support is a key factor in the preparation method. Optimizing the incipient wetness impregnation process led to the use of a packed column (plastic syringe barrel) of the intended support through which an aqueous solution of cobalt nitrate was flushed under gravity, which gave a homogeneous material as confirmed by the metal content analysis using ICP-OES.

In preparing an active Co-based supported catalyst for APFTS, an "*ex situ*" reduction proved to be a necessary step (350 °C at 5 °C / minute inside a furnace and under a hydrogen/nitrogen (50/50) atmosphere at a flow rate of 60 mL/min) after impregnation and calcination. Before catalytic testing, suspensions of 5% Co/SiO_2, 5% Co/Al_2O_3 and 10% Co/SiO_2 catalyst samples mixed with water were reduced "*in situ*" inside the reactor system at 150 °C for 2 h under H_2 gas at 14 bar. These suspensions did not show catalytic activity after they were tested for APFTS at 190 °C at 20 bar. Subsequently, the same catalyst samples, 5% Co/SiO_2, 5% Co/Al_2O_3 and 10%Co/SiO_2, were each reduced "*ex situ*" at 350 °C for 12 h under a H_2/N_2 atmosphere. The catalysts were then mixed with water forming a suspension, which was then reduced "*in situ*" inside the reactor system at 150 °C for 2 h under H_2 gas at 14 bar. After APFTS testing, these samples showed activity confirmed by the formation of both C_1 and C_2 hydrocarbons observed *via* gas

product analysis by gas chromatography. The effect of the elimination of the "*in situ*" reduction after conducting an "*ex situ*" reduction was not explored in the present report, but it is an aspect that could be explored in the future. The "*ex situ*" reduction is suggested to be a critical step for the formation of Co^0 active sites necessary for the preparation of a catalyst that could be used for APFTS. The inefficiency of only conducting the "*in situ*" reduction at 150 °C for 2 h could be explained by the use of a low temperature and possible interactions of the catalyst with the water.

Catalyst samples of 5% Co/SiO_2, 5% Co/Al_2O_3, 10% Co/SiO_2, 10% Co/Al_2O_3 and 25% Co/SiO_2 were tested for APFTS at 190 °C and 20 bar for 48 h, showing a low activity which could not be calculated by the difference in pressure before and after catalytic testing. The activity was confirmed by the formation carbon dioxide, methane, ethylene, and ethane observed after the gas product analysis by gas chromatography. Methane was the primary product obtained for all of the catalyst samples, showing the highest peak in the gas chromatograms. The formation of carbon dioxide was only observed when using catalyst with Al_2O_3 as a support. The formation of carbon dioxide was not further explored since reproducibility using SiO_2 was the primary focus, but it poses an important question as to the effect of Al_2O_3 as a support for the selectivity towards carbon dioxide when conducting APFTS. Methane, ethylene and ethane were observed as products when using a 10% Co/SiO_2 catalyst.

An estimated catalytic activity for one of the more active catalysts reported (10% Co/Al_2O_3) catalyst was found to be 1×10^{-3} mol_{CO} mol^{-1}_{Co} h^{-1}, calculated on the basis of the GC FID signal for methane. The catalytic activity reported is significantly low compared to values reported in literature for 0.5%Pt-25%Co/Al_2O_3 and Co NP catalysts. Differences in the catalyst preparation, the use of noble metal promoters, reactor systems for catalytic testing and temperature and pressure conditions for APFTS with literature results can amount for the low catalytic activity

reported here. The influence of Pt when used as a promoter for an Al_2O_3-supported catalyst can be explored in the future, since based on literature reports, APFTS can be performed using a Co-based catalysts using Al_2O_3 as a support, but the catalytic activity increases significantly when adding Pt to the catalyst to act as a promoter.

A crucial factor contributing to the catalytic activity when conducting APFTS is the reactor system used for the catalytic testing. As reported here in this thesis, the pressure of the reactant gasses is distributed from the input needle valve from where the reactant gases are flowed into the reactor system, all the way to the reactor tube. The suspension of the catalyst mixed with the water is located at the bottom of the reactor tube. It could be possible that during the catalytic synthesis, only a small volume of reactant gasses are in contact with the catalyst in the reaction zone. Minimum interaction between the reactant gases and the catalyst could amount for the low activity obtained. APFTS has been reported in literature by using a batch reactor system showing unprecedented activity,[7] as well as with a continuous flow reactor,[61] however details of the reactor designs are not further explained.

In summary, catalytic activity (albeit very low) was found for APFTS using conventional Co-based supported catalysts described in this thesis through detecting C_1 and C_2 products *via* gas chromatography and by obtaining a small pressure difference in the system over a catalytic test run. In the prior literature, APFTS had only been reported by using Co-based supported catalysts with the addition of promoters, so the work presented here represents a first step in trying to understand the catalytic process of the so-called APFTS.

5. Future Study

In future studies, the catalyst preparation method of Co-based supported catalysts should be examined using, for example slurry impregnation as performed by Pendyala *et al*.[63] Since an optimization of an incipient wetness impregnation was studied in this thesis using a packed column (plastic syringe), however a slurry impregnation can improve the metal precursor solution distribution. Co NP catalysts can also be prepared to determine the influence of oxide supports when conducting APFTS. Pendyala and coworkers reported a higher selectivity towards methane for a Pt-promoted Co-based catalyst, compared to that of unsupported and zeolite-supported ruthenium catalysts that the authors also used for APFTS. This suggests that interactions between the oxide support and the metal can account for a lower activity and a higher selectivity towards methane. Moreover, the use of noble metal promoters whilst using the reported catalyst preparation method could also be explored for comparison with activity values reported in literature for promoted Co-based catalysts used for APFTS. For example, Wang *et al*. observed an increase in the catalytic activity to 0.6 mol_{CO} mol^{-1}_{Co} h^{-1} on adding a small amount of Pt (molar ratio of Pt:Co = 0.05) to their unsupported Co nanoparticle catalyst system.[62]

The formation of carbon dioxide was only observed when using catalyst with Al_2O_3 as a support. The formation of carbon dioxide was not further explored since reproducibility using SiO_2 was the primary focus, but it poses an important question as to the effect of Al_2O_3 as a support for the selectivity towards carbon dioxide when conducting APFTS. In their paper Wigzell *et al*.[53] reported that when supported on Al_2O_3, cobalt nitrate reduction is catalyzed with by two events occurring below 350 °C, which is the same temperature used for the *ex situ* reduction used for the Co-based catalysts prepared for this thesis. In contrast, the SiO_2-supported complex exhibits reduction events that are all reduced in temperature relative to the unsupported salt (cobalt precursor). This suggests that there are significant differences in the reduction step for Al_2O_3- and SiO_2-supported catalysts, which can affect the product selectivity when conducting APFTS. The

influence of the *ex situ* reduction of a Co-based supported catalyst for APFTS can also be studied without conducting the *in situ* reduction and analyze the impact on the catalytic testing.

A subsequent step in understating APFTS could be made by optimizing the reactor system employed in the present report to improve the interaction of the catalyst suspended in water whilst using the methodology reported. If a higher activity could be obtained by this optimization and liquid products are obtained, the benefits of APFTS for product separation could be analyzed. Slurry phase reactors are suitable when conducting LTFT, and the operational temperature used in the present report fits in that classification of FTS.[18] Working on the reactor design for APFTS when using a conventional Co-based supported catalyst represents the main challenge for future work, to ensure good catalytic activity and understating in a more detailed way, the benefits conducting FTS in aqueous phases, or the so-called APFTS.

6. References

1 G. W. Huber, S. Iborra and A. Corma, *Chem.Rev.*, 2006, **106**, 4044–4098.

2 M. J. A. Tijmensen, A. P. C. Faaij, C. N. Hamelinck and M. R. M. Van Hardeveld, *Biomass and Bioenergy*, 2002, **23**, 129–152.

3 M. E. Dry, *Catal. Today*, 2002, **71**, 227–241.

4 R. L. Espinoza, A. P. Steynberg, B. Jager and A. C. Vosloo, *Appl. Catal. A Gen.*, 1999, **186**, 13–26.

5 B. Jager and R. Espinoza, *Catal. Today*, 1995, **23**, 17–28.

6 D. Leckel, *Energy & Fuels*, 2009, **23**, 2342–2358.

7 C. X. Xiao, Z. P. Cai, T. Wang, Y. Kou and N. Yan, *Angew. Chemie - Int. Ed.*, 2008, **47**, 746–749.

8 C. K. Rofer-Depoorter, *Chem.Rev.*, 1981, **81**, 447–474.

9 H. Schulz, *Appl. Catal. A Gen.*, 1999, **186**, 3–12.

10 C. H. Bartholomew and R. J. Farrauto, *Fundamentals of Industrial Catalytic Processes: Second Edition*, 2010.

11 B. H. Davis, *Catal. Today*, 2009, **141**, 25–33.

12 S. R. Craxford and E. K. Rideal, *J. Chem. Soc.*, 1939, 1604–1614.

13 J. T. Kummer and P. H. Emmett, *J. Am. Chem. Soc.*, 1953, **75**, 5177–5183.

14 J. T. Kummer, T. W. DeWitt and P. H. Emmett, *J. Am. Chem. Soc.*, 1948, **70**, 3632–3643.

15 H. H. Storch, N. Golumbic and R. B. Anderson, *John Wiley Sons, Inc, New York*.

16 B. H. Davis, *Fuel Process. Technol.*, 2001, **71**, 157–166.

17 J. V Underwood, *Ind. Eng. Chem.*, 1940, **32**, 449–454.

18 A. Y. Khodakov, W. Chu and P. Fongarland, *Chem. Rev.*, 2007, **107**, 1692–1744.

19 A. de Klerk, *Green Chem.*, 2008, **10**, 1237–1344.

20 D. J. Wilhelm, D. R. Simbeck, A. D. Karp and R. L. Dickenson, *Fuel Process. Technol.*, 2001, **71**, 139–148.

21 L. Barelli, G. Bidini, F. Gallorini and S. Servili, *Energy*, 2008, 33, 554–570.

22 A. Molina and F. Mondragón, *Fuel*, 1998, **77**, 1831–1839.

23 R. B. Anderson, R. A. Friedel and H. H. Storch, *J. Chem. Phys.*, 1951, **19**, 313–319.

24 G. Henrici-Olivé and S. Olivé, *Angew. Chemie Int. Ed. English*, 1976, **15**, 136–141.

25 I. T. Specific and M. A. Vannice, *J. Catal.*, 1975, **37**, 449–461.

26 C. H. Bartholomew, *AIChE Natl. Spring Meet.*, 2003, 83b.

27 J. J. C. Geerlings, M. C. Zonnevylle and C. P. M. de Groot, *Surf. Sci.*, 1991, **241**, 302–314.

28 V. G. H. Iglesia Enrique, Soled Stuart L., Fiato A. Rocco, *J. Catal.*, 1993, **143**, 345–368.

29 E. Iglesia, S. L. Soled and R. A. Fiato, *J. Catal.*, 1992, **137**, 212–224.

30 E. Iglesia, S. C. Reyes, R. J. Madon and S. L. Soled, *Adv. Catal.*, 1993, **39**, 221–302.

31 S. L. Soled, E. Iglesia, S. Miseo, B. A. Derites and R. A. Fiato, *Top. Catal.*, 1995, **2**, 193–205.

32 E. Iglesia, *Appl. Catal. A Gen.*, 1997, **161**, 59–78.

33 T. Ishihara, K. Eguchi and H. Arai, *J. Mol. Catal.*, 1992, **72**, 253–261.

34 S. Bessell, *Appl. Catal. A, Gen.*, 1993, **96**, 253–268.

35 R. C. Reuel and C. H. Bartholomew, *J. Catal.*, 1984, **85**, 78–88.

36 A. M. Saib, M. Claeys and E. van Steen, *Catal. Today*, 2002, **71**, 395–402.

37 D. Song and J. Li, *J. Mol. Catal. A Chem.*, 2006, **247**, 206–212.

38 W. J. Wang and Y. W. Chen, *Appl. Catal.*, 1991, **77**, 223–233.

39 R. L. Chin and D. M. Hercules, *J. Phys. Chem.*, 1982, **86**, 360–367.

40 J. Zhang, J. Chen, J. Ren and Y. Sun, *Appl. Catal. A Gen.*, 2003, **243**, 121–133.

41 Y. Zhang, H. Xiong, K. Liew and J. Li, *J. Mol. Catal. A Chem.*, 2005, **237**, 172–181.

42 R. Bechara, D. Balloy and D. Vanhove, *Appl. Catal. A Gen.*, 2001, **207**, 343–353.

43 J. A. Schwarz, *Catal. Today*, 1992, **15**, 395–405.

44 G. A. Parks, *Chem. Rev.*, 1965, **65**, 177–198.

45 Y. Zhang, K. Hanayama and N. Tsubaki, *Catal. Commun.*, 2006, **7**, 251–254.

46 L. Guczi, D. Bazin, I. Kovács, L. Borkó, Z. Schay, J. Lynch, P. Parent, C. Lafon, G. Stefler, Z. Koppány and I. Sajó, *Top. Catal.*, 2002, **20**, 129–139.

47 A. Kogelbauer, J. G. Goodwin and R. Oukaci, *J. Catal.*, 1996, **160**, 125–133.

48 N. Tsubaki, S. Sun and K. Fujimoto, *J. Catal.*, 2001, **199**, 236–246.

49 K. Shimura, T. Miyazawa, T. Hanaoka and S. Hirata, *Appl. Catal. A Gen.*, 2015, **494**, 1–11.

50 a. M. Hilmen, D. Schanke and a. Holmen, *Catal. Letters*, 1996, **38**, 143–147.

51 J. S. Girardon, A. Constant-Griboval, L. Gengembre, P. A. Chernavskii and A. Y. Khodakov, *Catal. Today*, 2005, **106**, 161–165.

52 J. S. Girardon, A. S. Lermontov, L. Gengembre, P. A. Chernavskii, A. Griboval-Constant and A. Y. Khodakov, *J. Catal.*, 2005, **230**, 339–352.

53 F. A. Wigzell and S. D. Jackson, *Appl. Petrochemical Res.*, 2017, **7**, 9–21.

54 A. K. Dalai and B. H. Davis, *Appl. Catal. A Gen.*, 2008, **348**, 1–15.

55 N. Yan, C. Zhao, C. Luo, P. J. Dyson, H. Liu and Y. Kou, *J. Am. Chem. Soc.*, 2006, **128**, 8714–8715.

56 C. Zhao, H. zhi Wang, N. Yan, C. xian Xiao, X. dong Mu, P. J. Dyson and Y. Kou, *J. Catal.*, 2007, **250**, 33–40.

57 C. xian Xiao, H. zhi Wang, X. dong Mu and Y. Kou, *J. Catal.*, 2007, **250**, 25–32.

58 X. D. Mu, J. Q. Meng, Z. C. Li and Y. Kou, *J. Am. Chem. Soc.*, 2005, **127**, 9694–9695.

59 J. Schulz, A. Roucoux and H. Patin, *Chem. - A Eur. J.*, 2000, **6**, 618–624.

60 X. Y. Quek, Y. Guan, R. A. VanSanten and E. J. M. Hensen, *ChemCatChem*, 2011, **3**, 1735–1738.

61 L. T. Liu, G. Sun, C. Wang, J. H. Yang, C. X. Xiao, H. Wang, D. Ma and Y. Kou, *Catal. Today*, 2012, **183**, 136–142.

62 H. Wang, W. Zhou, J.-X. Liu, R. Si, G. Sun, M.-Q. Zhong, H.-Y. Su, H.-B. Zhao, J. a Rodriguez, S. J. Pennycook, J.-C. Idrobo, W.-X. Li, Y. Kou and D. Ma, *J. Am. Chem. Soc.*, 2013, **135**, 4149–4158.

63 V. R. R. Pendyala, W. D. Shafer and B. H. Davis, *Catal. Letters*, 2013, **143**, 895–901.

64 F. Diehl and A. Y. Khodakov, *Oil Gas Sci. Technol.*, 2009, 64, 11–24.